Journal of Controlled Release 272 (2018) 169–181

Contents lists available at ScienceDirect

Journal of Controlled Release

journal homepage: www.elsevier.com/locate/jconrel

Review article

Mechanistic understanding the bioeffects of ultrasound-driven microbubbles to enhance macromolecule delivery

Peng Qin[a,*], Tao Han[a], Alfred C.H. Yu[b], Lin Xu[c]

[a] Department of Instrument Science and Engineering, Shanghai Jiao Tong University, Shanghai, China
[b] Department of Electrical and Computer Engineering, University of Waterloo, Waterloo, ON, Canada
[c] National Key Laboratory of Plant Molecular Genetics, CAS Center for Excellence in Molecular Plant Sciences, Institute of Plant Physiology and Ecology, Shanghai Institutes for Biological Sciences, Chinese Academy of Sciences, Shanghai, China

ARTICLE INFO

Keywords:
Ultrasound
Microbubbles
Cavitation
Bioeffects
Macromolecule delivery

ABSTRACT

Ultrasound-driven microbubbles can trigger reversible membrane perforation (sonoporation), open interendothelial junctions and stimulate endocytosis, thereby providing a temporary and reversible time-window for the delivery of macromolecules across biological membranes and endothelial barriers. This time-window is related not only to cavitation events, but also to biological regulatory mechanisms. Mechanistic understanding of the interaction between cavitation events and cells and tissues, as well as the subsequent cellular and molecular responses will lead to new design strategies with improved efficacy and minimized side effects. Recent important progress on the spatiotemporal characteristics of sonoporation, cavitation-induced interendothelial gap and endocytosis, and the spatiotemporal bioeffects and the preliminary biological mechanisms in cavitation-enhanced permeability, has been made. On the basis of the summary of this research progress, this Review outlines the underlying bioeffects and the related biological regulatory mechanisms involved in cavitation-enhanced permeability; provides a critical commentary on the future tasks and directions in this field, including developing a standardized methodology to reveal mechanism-based bioeffects in depth, and designing biology-based treatment strategies to improve efficacy and safety. Such mechanistic understanding the bioeffects that contribute to cavitation-enhanced delivery will accelerate the translation of this approach to the clinic.

1. Introduction

The purpose of a drug delivery system is to transport therapeutic agents across biological membranes and endothelial barriers, and improve the efficacy of therapeutics at the specific disease sites while reducing undesired side effects [1]. Ultrasound-based approach has been reported to facilitate the transport of membrane impermeable compounds into cells and tissues via thermal (hyperthermia) or mechanical mechanisms [2]. When the rate of ultrasound energy deposition exceeds thermal diffusion or transduction in tissue, the temperature rises and thereby generates cellular changes [3]. Hyperthermia has been shown to enhance vascular permeability for assisting macromolecules delivery into tissues [4,5]. However, the used high intensity ultrasound in hyperthermia can produce rapid local temperature increase and cause unpredictable and irreversible damage [6,7]. The travelling ultrasound also causes a rapid change of pressure and fluid velocity in the tissue, producing shear stress and other mechanical effects [8], which could be amplified by the artificial gas-filled microbubbles [9–11]. Under the influencing of the alternating positive and negative acoustic pressure, microbubbles undergo stable oscillation (expansion and contraction), followed by growth, large-amplitude oscillation (i.e. stable cavitation) and, finally, violent collapse (i.e. inertial cavitation) [12,13]. Oscillating microbubbles set the surrounding liquid into motion, forming microstreaming, which induces shear stress on adjacent objects [14,15]. Violently collapsing microbubbles send out shockwaves and produce a directed jet in the fluid [16–18]. The interaction of these two kinds of cavitation with cells or tissues can induce reversible perforation on the plasma membrane [19–21], opening interendothelial junctions (forming interendothelial gap) [22,23] and stimulating endocytosis [24,25], as illustrated in Fig. 1. These bioeffects can overcome the barriers of the vessel wall and plasma membrane by initiating active or passive transport, and facilitate delivery of impermeable compounds into the targeted region [26]. Since the used low intensity ultrasound for driving bubbles can noninvasively target a tissue volume at depth without affecting the surrounding soft tissue, and the effects caused by ultrasound may be spatially and temporally controlled, this approach is currently attracting considerable research interest [12].

* Corresponding author.
E-mail address: pqin@sjtu.edu.cn (P. Qin).

https://doi.org/10.1016/j.jconrel.2018.01.001
Received 12 October 2017; Received in revised form 2 January 2018; Accepted 3 January 2018
Available online 04 January 2018

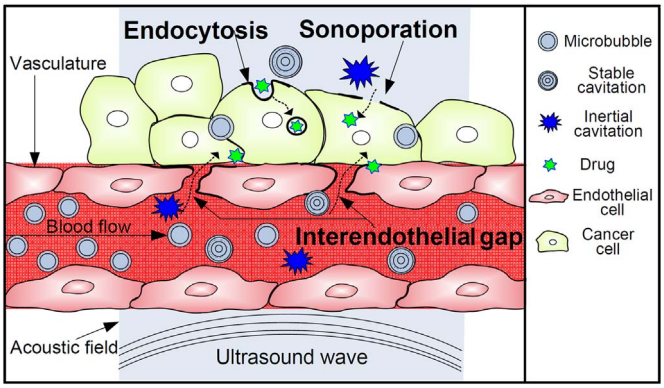

Fig. 1. Overview of the three main passive and active delivery routes enhanced by ultrasound-driven microbubbles. Sonoporation, which refers to transient and reversible membrane perforation by acoustic cavitation, allows macromolecules to passively diffuse into the cell. The interendothelial gap, which refers to the alteration of vascular integrity and the opening of the interendothelial junction by acoustic cavitation, provides an active route for macromolecule delivery into the extravascular tissues. Endocytosis enhanced by stable cavitation can actively delivery the macromolecules into the cell via vesicles.

The basic framework and principles of this approach have been established in previous in vitro and in vivo work. The feasibility and potential of this method has been demonstrated for the delivery of therapeutic agents, antibodies and other agents into targeted tissues [27]. Some summaries of in vitro and preclinical studies are listed in Table 1. However, besides the above bioeffects for macromolecule delivery, a variety of unwanted bioeffects, including hemorrhage, extensive cell death or even thrombosis, are found after cavitation treatment [40,41]. Further, although cavitation treatment is devoid of long-term cumulative effects, this approach might induce long-term adverse bioeffects on the targeted tissues [3,42]. These deleterious bioeffects may be a stumbling block for the clinical applications of this approach. On the other side, the overall delivery efficacy of a drug treatment is dependent on the amount of the affected cells, the concentration, distribution and depth of the drug penetration into the targeted tissues [43,44]. Since the cavitating bubbles is obstructed by the internal elastic lamina of the vasculature and limited to superficial cell layers, only a minority of the cell population could achieve intracellular uptake [45]. The interstitial space with densely arranged cells and elastic fiber also limits the depth of penetration into tissues [2]. Thus, achieving satisfactory efficacy and safety is a big challenge for moving this approach from the bench to beside.

Surveying the existing reports about cavitation-enhanced delivery, we found that the increased permeability that results from sonoporation, interendothelial gap and endocytosis is temporary and reversible, lasting from a few seconds to a few hours. This temporal window for macromolecule delivery is dependent on not only cavitation activities (related to ultrasound parameters, microbubble properties and flowing environments), but also biological regulatory mechanisms (required for membrane resealing, junction restoration and physiological recovery).

Table 1
Summaries of the studies on cavitation-enhanced macromolecule delivery.

Tissue target	Therapeutic macromolecules	Ultrasound-driven microbubbles	Bioeffects	Publications
MRC-5 fetal fibroblasts cells	No	1 MHz, 10 μs 0.85 MPa PRF Targestar microbubbles	Sonoporation	Hu et al. [21]
Human embryonic kidney cells	Impermeable propidium iodide	1.25 MHz, 2.4–8 μs, 0.17–0.60 MPa, Targestar microbubbles	Sonoporation	Fan et al. [28]
Human umbilical vein endothelial cells	Impermeable propidium iodide	0.5, 1 and 2 MHz 0.1–0.8 MPa PRF SonoVue microbubbles	Interendothelial junction opening	Helfield et al. [23]
A small vessel	No	1 MHz, 0.8 or 1 MPa PRF, microbubbles	Interendothelial gap formation	Caskey et al. [29]
Human melanoma cells	FITC-dextran (4 KDa and 2 MDa)	1 MHz, 0.1–0.5 MPa PRF, 2000 cycles 125 Hz PRF for 5 s, lipid microbubbles	Endocytosis	Cock et al. [30]
Melanoma cells	SYTOX-Green	1 MHz, 0.5,1 and 2 W/cm^2 for 60 s, BR14 bubbles	Endocytosis	Zeghimi et al. [31]
BBB of a pig model	Lipid-encapsulated microbubbles	1 MHz, 100 Hz PRF, 2 ms PD	Evans blue extravasation across BBB	Xie et al. [32]
The rat brain	DOX hydrochloride-encapsulated	1.5/1.7 MHz, 0.36–2.5 MPa, 1 Hz PRF, 1% DC, 30 s, Optison microbubbles	The increase of the permeability of DOX across BBB	Treat et al. [33]
The mouse brain	Herceptin (monoclonal antibodies)	0.69 MHz, 0.6/0.8 MPa	Herceptin delivered into the brain	Kinoshita et al. [34]
The rat heart	Luciferase	1.3 MHz, MI = 1.5 4 cycles, lipid-shelled bubbles, octafluoropropane	Increased luciferase expression in heart tissue	Bekeredjia et al. [35]
Porcine carotid	Anti-actin-ELIP	1.0 MHz, CW, 0.23 MPa	ELIP penetration into tunica media	Laing et al. [36]
Subcutaneous murine ovarian carcinoma tumor	Plasmid encoding interleukin 12 driven by CMV promoter	1.0 MHz, CW, 0.7 W/cm^2 for 2 min liposomes with gas core	80% complete regression after repetitive treatment	Suzuki et al. [37]
Subcutaneous melanoma tumor xenograft	Plasmid encoding interferon β, CMV promoter	1.0 MHz, CW, 0.22 W/cm^2, 50% DC for 3 min, Sonazoid	Significant reduced tumor growth ratio after repetitive treatment	Yamaguchi et al. [38]
Subcutaneous prostate carcinoma xenograft	Antisense oligodeoxynucleotide directed against androgen receptor	1.75 MHz, color Doppler mode, MI 1.9, 9 min	Reduction of tumor growth	Haag et al. [39]

Therefore, it is possible to improve efficacy and minimize side effects by controlling cavitation activities and designing biological regulatory strategies. Recent studies achieved encouraging progress towards understanding the dynamic interactions of cavitating microbubbles with cells/tissues and spatiotemporally monitoring cavitation activities in the targeted region [19,46]. However, due to the complexity of biological tissue, besides plasma membrane perforation, interendotherlial gap formation and endocytosis, other cellular (e.g., intracellular Ca^{2+}, cytoskeleton and other organelles) and molecular (e.g., proteins related to membrane resealing, gap restoration and cell fate) responses in different spatial and temporal scales may be triggered by ultrasound-driven microbubbles, thereby affecting the kinetics of cavitation-enhanced permeability and cell fate trends. As such, achieving mechanistic understanding the bioeffects involved in cavitation-enhanced permeability is key to ensure that translation of this approach are efficiently and safely executed [2,47,48].

This Review provides a summary of these significant investigations and a critical perspective on the challenge and future directions in this field. More importantly, this Review also surveys the plausible biological regulatory mechanisms on membrane perforation and resealing, interendothelial gap formation and closure, and endocytosis enhancement post-cavitation; and discusses the potential implications of leveraging an understanding of these biological mechanisms for improving efficacy and biosafety. Such a mechanistic understanding of the bioeffects in cavitation-enhanced permeability could facilitate the translation of this technique to the clinic.

2. Sonoporation elicited by acoustic cavitation

Sonoporation refers to transiently reversible membrane perforation elicited by ultrasound-driven microbubbles. This entails two sequential biophysical processes: membrane perforation by the mechanical effects of cavitation and pore resealing through biological mechanisms [49–51].

2.1. Spatiotemporal characteristics of pore formation

2.1.1. Time points of pore formation

Elegant in vitro high-speed photography and fluorescence microscopy studies provided a clear understanding of the dynamics of membrane perforation and cell–microbubble interactions during cavitation. Nico et al. used a real-time ultrafast transmission microscope to demonstrate that stable oscillation of microbubbles induced by 1 MHz ultrasound with 0.4 MPa peak negative pressure (PNP) could gently push and pull the membrane as a result of mechanical stress, leading to rapid membrane deformation and perforation after sonication for 5 s [20]. Using a real-time microscopy, moving cavitating microbubbles drived by 0.834 MHz ultrasound with 0.12 MPa PNP were found to cause membrane deformation through microstreaming-induced shear stress [52]. Fan et al. showed that bubble fragments formation under 10 μs and 0.24 MPa PNP exposure caused the instantaneous increase of intracellular propidium iodide (PI) uptake and continuous increase for about 2 min [28,53]. Kudo et al. used a high-speed camera to determine that intracellular PI uptake occurred almost synchronously with microjet formation from non-uniform contraction of bubbles, which were triggered by a 3 μs ultrasound burst with 1.1 MPa PNP [54]. Hu et al. used confocal fluorescence microscopy to observe the immediate formation of localized membrane perforation after applying a 10 μs ultrasound pulse with 0.85 MPa PNP to cause microbubble collapse [21]. These single-cell experiments indicate that when microbubbles are exposed to ultrasound pulses, membrane perforation occurs within several to tens of microseconds, almost synchronously with stable or inertial cavitation.

2.1.2. Spatial characteristics of membrane pores

The spatial characteristics of membrane perforation, including the size and the location of pores on the plasma membrane, are mainly correlated with the PNP and non-acoustic (e.g. bubble-related and bubble–cell-related) parameters.

Recent studies have revealed that membrane perforation does not occur until microbubbles are close to the cell membrane, suggesting the importance of the bubble–cell distance (d) for cavitation-perforated membrane. Ward first observed the relationship between d and the sonoporation efficiency in 2000 [55]. Le Gac et al. studied the critical distance for membrane perforation on a single cell, and determined that membrane perforation occurred with 75% probability when d was equal to 75% of the maximum bubble radius [56]. Zhou et al. found the shockwave from inertial cavitation evoked membrane perforation when the ratio of d to the bubble diameter (D) was < 0.75 [57]. Qin et al. revealed the importance of d in sonoporation using real-time microscopy at the single-cell level. When d is less than D, microbubble collapse was found to cause localized membrane perforation, the extent of which positively correlated with d[58]. Owing to the importance of d in sonoporation, several physical and biochemical strategies were proposed to bring bubbles close to the targeted cell to achieve the critical distance for sonoporation. For example, low-pressure (50 kPa) and long-duration (3.3 s) pulses were used to generate primary radiation forces, which pushed bubbles to the surface of the cell. High-pressure (2 MPa) pulses with short duration (3.3 μs) were then used to induce bubble collapse [59]. Other alternative biochemical methods involve conjugating a specific ligand or antibody to microbubbles, which then attach to the surface of the targeted cells [32,60]. These methods have been demonstrated to improve the delivery efficiency.

Pore sizes are closely related to the PNP below the critical value of d. Real-time observation of pore size provides more convincing results than methods (such as scanning electron microscopy and atomic force microscopy) used for measuring pore sizes in samples post-exposure. Fan and Zhou et al. estimated the pore diameter may be as small as 10–100 nm by fitting the intracellular diffusion to a quasi-steady-state electro-diffusion model and by measuring the maximal transmembrane current via the patch-clamp technique after bubble exposure to 2.4 μs ultrasound with 0.12 or 0.3 MPa PNP [28,61]. In another example, Kudo et al. determined, using electron microscopy, large membrane perforation up to 1 μm after 1.1 MPa PNP exposure [54,62]; a similar pore size was observed by Hu et al. using 0.85 MPa PNP [21]. In general, the pore size induced by low PNP ranged from several tens to a few hundred nanometers [24,63,64], whereas high PNP elicited membrane perforation up to the micron scale [21,28,65,66]. Moreover, according to the intracellular PI uptake level, the sonoporated cells are categorized into different types, which may be related to the fate in short- and long-term post-exposure. These findings suggest that membrane perforation can be spatially and temporally well controlled (for example, by adjusting the PNP, pulse duration) for improving delivery efficacy while avoiding permanent cellular damage [28,67].

2.2. Kinetics of perforated membrane resealing

The time-varying pore morphology was determined by the following methods. The patch-clamp technique was used to show that pores close within seconds after switching off the ultrasound [51]. Hu et al. used real-time confocal microscopy to observe the completion of pore closure on the order of tens of seconds, and pointed out that the perforation sites within the spatial peak area ($< 30\ \mu m^2$) successfully resealed, whereas large perforation areas ($> 100\ \mu m^2$) failed to reseal [21]. In other studies, the perforated membrane was shown, through temporal changes of an internalized impermeable marker, to completely reseal within about 100 s [28,57,58]. The rapid restoration of the intracellular calcium level and membrane potential also suggested that resealing of the perforated membrane was complete within about 100 s [68,69]. Further, the number of permeant structures on the membrane after sonoporation was characterized as function of time by exponential decay with a half-life close to 10 min. One hour after

sonoporation, most cells exhibited a full recovery to their native membrane integrity [19]. These findings indicate different kinetics of membrane resealing, ranging from the order of milliseconds to minutes depending on the degree of perforation.

2.3. Bioeffects triggered by sonoporation

1) *Intracellular Ca^{2+} transients*. Intracellular Ca^{2+} post-cavitation is quantified by measuring the fluorescence of a Ca^{2+} probe using a real-time fluorescence microscope. For example, The intracellular Ca^{2+} concentration was found to be synchronously increased with the onset of sonoporation, and reached a peak value quickly (within 5–10 s), then gradually returned to the equilibrium level within approximate 100 s. The presence of these ultrashort Ca^{2+} transients was temporally correlated with the occurrence of sonoporation, and the amplitude was correlated with the degree of sonoporation [69]. Relatively lower amplitude of delayed Ca^{2+} transient was observed in the non-sonoporated cells, which were spatially adjacent to the perforated cells [70,71]. Similar short-term changes in intracellular Ca^{2+} concentration were also found in cardiomyocytes and endothelial cells exposed to ultrasound in the presence of microbubbles [72,73]. Moreover, Honda et al. observed the rapid increase in intracellular Ca^{2+}, and subsequent recovery to normal levels in the long-term (about 4 h) post-exposure [74]. Future studies are needed to explain these different Ca^{2+} transient patterns and correlate this to the long-term cell fate post exposure.
   It is currently thought that the intracellular Ca^{2+} transients are mainly due to the concentration-driven passive diffusion of Ca^{2+} through the perforated membrane [70,71]. Juffermans et al. demonstrated that Ca^{2+} influx did not occur via the L-type Ca^{2+} channel by using the ion-channel blocker verapamil [72,73]. The recovery of intracellular Ca^{2+} may be the result of complex biochemical processes, including active extracellular efflux, protein buffering, and storage in the sarcoplasmic reticulum and mitochondria [69]. However, the delayed increase and oscillation of the Ca^{2+} transient may be caused by intracellular conduction mechanisms, such as the generation of inositol phosphate, or the subsequent release of Ca^{2+} from the endoplasmic reticulum [75–77]. More importantly, because cells undergo immediate lysis when the Ca^{2+} concentration exceeds 10 μM [78], it is crucial to know the intracellular Ca^{2+} profile within the period from sonication until the occurrence of apoptosis and the reason for intracellular Ca^{2+} dynamics post-exposure.
2) *Membrane potential change*. Intracellular Ca^{2+} transients may cause an imbalance of trans-membranous ions, thereby altering the cellular electrophysiology dynamics. Deng et al. carried out the first electrophysiology measurements on a patch-clamped *Xenopus* oocyte during 0.29-MPa ultrasound exposure to microbubbles. They observed a slightly delayed inward electric current, which proceeded to increase in amplitude before recovering to a normal level at the end of exposure [51]. This finding suggests that enhanced membrane permeability facilitates transmembrane ion flux and affects the membrane potential. Oscillating microbubbles at low PNP could cause the hyperpolarization of the membrane potential, which most likely occurs through an indirect process in which Ca^{2+} transients activate Ca^{2+}-gated ion channels, such as BKca channels, to trigger K^+ efflux [79–81]. Inhibition of BKca channels and thus blocking K^+ efflux was found to cause a very slight depolarization of the membrane potential at 50-kPa PNP owing to the small Ca^{2+} influx [79,81]. However, at 250 kPa PNP, blockage of BKca channels led to a high membrane depolarization owing to massive Ca^{2+} influx [79,81].
   The membrane potential in Hela cells, which are naturally deficient in voltage-gated ion channels, exhibited heterogeneous depolarization after 20 μs ultrasound exposure with 0.5 MPa PNP in the presence of microbubbles [68]. In the reversibly sonoporated cells, the membrane potential rapidly decreased to a minimum value within ~60 s, and then gradually recovered to a normal level after ~120 s, or was sustained at a relatively low level (at least 10 min). The membrane potential of the irreversibly sonoporated cells was permanently reduced. Intact cells adjacent to sonoporated ones also underwent delayed and transitory membrane depolarization similar to the delayed Ca^{2+} influx [68]. The change in membrane potential observed in these studies indicates a disturbance of the concentrations of intra- and extracellular ions. In terms of biosafety, it is essential to investigate how the long-term fate of reversibly sonoporated cells responses to the early membrane potential changes.
3) *Homeostasis of reactive oxygen species (ROS)*. An appropriate quantity of ROS is necessary to maintain normal physiological function. However, imbalance between oxidants and antioxidants may produce adverse effects. It is known that shear stress from bubble oscillation leads to the formation of H_2O_2 and superoxide [14,82]. For example, the level of intracellular H_2O_2 markedly increases about 1 h after exposure to ultrasound with low PNP (0.1–0.2 MPa). When catalase was added to inhibit the intracellular H_2O_2, Ca^{2+} influx was blocked immediately following exposure, suggesting a close relationship between Ca^{2+} influx and H_2O_2 production [72]. Our recent unpublished results indicate that ROS in sonoporated cells rapidly decreases within ~100 s post-exposure owing to extracellular passive diffusion of ROS indicator through the perforated membrane. This process was similar to the influx of extracellular PI. In the following 260 s, the ROS level in the sonoporated cells gradually increased, correlating positively with the degree of sonoporation. However, the origin of intracellular ROS and the relationship between intracellular ROS and the long-term cell fate of the cells remain unknown.
4) *Cytoskeleton dynamics*. The cytoskeleton, one of main mechanoconduction pathways, converts mechanical signals presented at the cell membrane into intracellular biochemical signals. Previous studies determined that oscillatory strains from pulsed ultrasound with 0.17–0.29 MPa PNP promoted the fluidization of the cytoskeleton within ~3 min post-exposure [83,84]. In the presence of microbubbles, when cells were exposed to ultrasound with 0.1 MPa PNP, F-actin stress fibers were observed to spatially rearrange and mainly gather at the center of the cells; the fibers then returned to a uniform distribution at ~30 min post-exposure [85]. However, these studies did not track the occurrence of sonoporation or the spatiotemporal characteristics of cytoskeleton changes. When the cells were exposed to violently collapsing microbubbles, F-actin was immediately ruptured with spatiotemporal correlation with the perforation of the membrane [86]. In the following 60 min, the F-actin fibers further disassembled, but the globular actin accumulated [86]. However, the findings described above only provide preliminary insight into the changes in the cytoskeleton upon sonoporation. The way in which the cytoskeleton responds to cavitation events and its role in the perforated membrane resealing remain unclear.

2.4. Mechanisms of resealing cavitation-perforated membranes

Sonoporated cells gradually recover to their pre-exposure state by two sequential biological processes: membrane resealing and cell recovery. The former refers to the rapid and short-term (several minutes) closure of perforation sites, whereas the latter refers to the long-term (several hours post-exposure) return of the cell physiology to its initial state, as shown in Fig. 2. It is essential to understand and regulate these biological processes to improve the efficacy and biosafety of sonoporation-based delivery. In this sub-section, we focus on known and possible mechanisms of resealing perforated membranes.

2.4.1. Ca^{2+}-dependent exocytosis

Sonoporation is inherently heterogeneous owing to the effects of the different types of cavitation (i.e. stable and inertial) and the

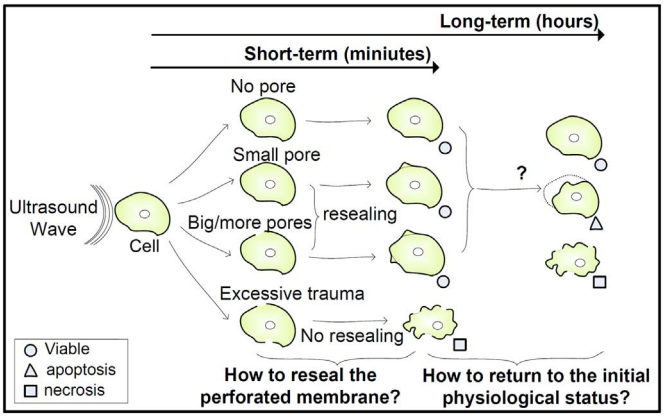

Fig. 2. Schematic representation of the relationship between the degree of membrane perforation and the short- and long-term cell fate.

inhomogeneous cavitation dose throughout the targeted region [24,63,64,87]. The repair of large or small pores may depend on different cellular mechanisms [88,89], as illustrated in Fig. 3. This would explain the identification in previous studies of contradictory biological events (such as exocytosis and endocytosis) that are involved in the resealing of cavitation-perforated membrane. It is also worth noting that although small pores (tens of nanometers) might be passively resealed owing to the inherent qualities of lipid bilayers and large pores (from hundreds of nanometers to microns) by exocytic patch formation, both the internal membrane and the delivery of the internal membrane to the plasma membrane by exocytosis are necessary for these two mechanisms [90,91].

Early studies revealed that chelating extracellular Ca^{2+} could terminate the resealing process, leading to cytosol loss and cell death, suggesting the essential role of Ca^{2+} in the membrane repair of sonoporated cells [51,69,72]. Moreover, the membrane fusion reaction for large wounds requires a higher Ca^{2+} threshold than that for the repair of small lesions [90]. Schlicher et al. used transmission electron microscopy to observe blebs and patch formation at the perforation sites of sonoporated cells, which temporally correlated with a decrease in

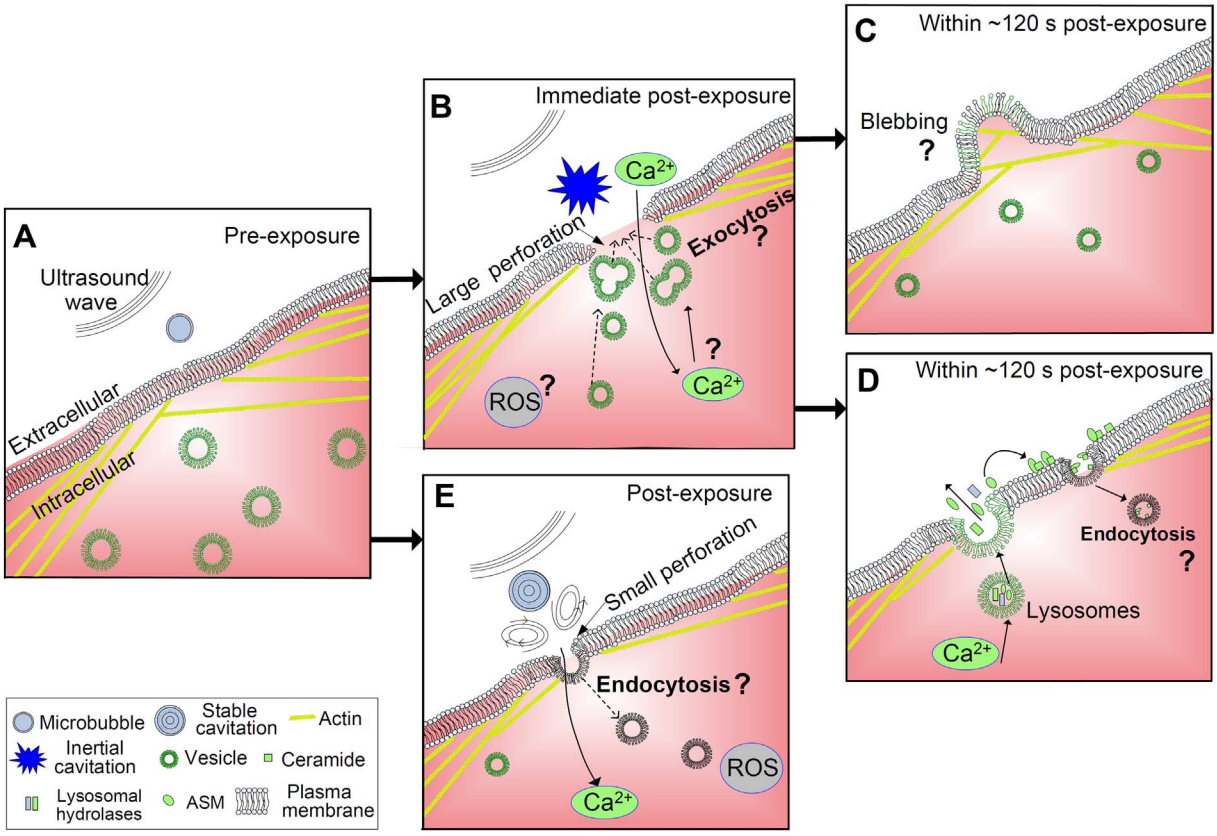

Fig. 3. Overview of possible mechanisms for the resealing of perforated membrane by ultrasound-driven microbubbles. (A) A cell with a lipid bilayer underlying the cytoskeleton and intracellular vesicles pre-exposure. (B) Inertial collapse of microbubbles causes a large membrane perforation. Extracellular calcium passively diffuses into the cytosol, forming calcium influx, which may initiate depolymerization of the actin and trigger exocytosis of intracellular vesicles (lysosomes, endosomes or Golgi). The fusion of exocytotic vesicles forms a patch to reseal perforation, forming blebbing at the site of the perforation (C). (D) Peripheral lysosomes fuse with the plasma membrane, releasing their contents extracellularly. Lysosomal acid sphingomyelinase (ASM) converts sphingomyelin into ceramide, causing membrane invagination and endosomes formation to reseal pore. (E) The small membrane perforation caused by oscillating bubbles can be removed by endocytosis owing to calcium influx.

fluorescence of labeled intracellular vesicles [92]. These findings suggest that vesicle trafficking is involved in pore resealing. However, these early studies don't elucidate the spatiotemporal characteristics of vesicles and the temporal relationship between intracellular Ca^{2+} and exocytosis of vesicles in the resealing of the perforated membrane.

Membrane-bound and Ca^{2+}-sensitive exocytic compartments mainly include Golgi, endoplasmic reticulum, early endosomes, late endosomes and lysosomes [90,93]. An open question relates to which internal membranes are delivered to the membrane surface by exocytosis, and then fuse with the plasma membrane to facilitate resealing. Previous studies indirectly found using the immunostaining method that the luminal domain Lamp-1 of the lysosome inserted the surface of the perforated membrane [94], suggesting that lysosomes may be the main vesicles capable of rapid exocytosis in response to elevated Ca^{2+} concentrations, as showed in Fig. 3B. However, these studies do not provide spatiotemporal evidence for the involvement of lysosomes in the resealing of sonoporated cells.

2.4.2. Endocytosis

Some studies have indicated that nanoscale membrane disruption by stable cavitation might be removed by endocytosis [19,95]. According to membrane resealing theory, there is a rapid and substantial formation of vesicles through endocytosis (i.e. invagination of the plasma membrane and accumulation close to the injury site) [96,97], as showed in Fig. 3E. Therefore, endocytosis is considered to reseal the membrane, thus compensating exocytosis. Further, lysosomes, which include > 50 different hydrolases, are delivered and fuse to the wound by rapid exocytosis [98]. Acid sphingomyelinase contained in lysosomes is released to the external environment by some hydrolases, where it extracellularly generates ceramide-enriched domains on the cell surface. Ceramide can induce endocytosis and rapid formation of endosomes [97]. The homotypic fusion of endocytic vesicles promotes membrane resealing. This resealing process is shown in Fig. 3D. Moreover, Ca^{2+} can also directly stimulate endocytosis for membrane resealing [91]. Whether the above mechanisms are involved in the resealing of cavitation-perforated membranes needs to be confirmed.

2.4.3. The role of the cytoskeleton

Rearrangement or disassembly of cortical actin filaments occurs during exocytosis. Previous studies found that the cytoskeleton was disassembled, disrupted and rearranged in sonoporated cells, and that this was associated with membrane deformation [83,84,86]. Some mechanosensors, such as integrins and stretch-activated ion channels, which link extracellular matrix molecules to the actin skeleton, can sense these changes and influence the endocytotic or exocytotic activity via intracellular signaling pathways [99,100]. However, it is still unknown how these pathways conduct and how this rearrangement of the cytoskeleton is spatiotemporally correlated with the resealing of perforated membranes. Moreover, single membrane blebs have been observed at the sites of small pores (as shown in Fig. 3C), whereas many blebs are dispersed around the membrane near large perforations [101]. The mechanism by which the cell identifies the degree of perforation and takes a particular course of exocytotic action to repair these lesions remains unclear. Specifically, it is unknown which components of the cytoskeleton assist the directional transport of intracellular vesicles to the perforation site, thereby forming blebs. Similarly, it is unclear which proteins assist in the delivery of vesicles along the cytoskeleton. Answering these questions will help provide strategies for regulating the short-term fate of sonopoated cells.

3. Interendothelial junction opened by acoustic cavitation

Ultrasound-driven microbubbles can temporarily alter the vascular integrity or open the interendothelial junction, thereby forming interendothelial gap, which provides another effective route for macromolecular delivery into extravascular tissue. Similar to the dynamics of membrane perforation and resealing, two different biological events, junction opening and restoration between endothelial cells, are observed after cavitation exposure.

3.1. Spatiotemporal characteristics of the opening and closing of the interendothelial junction

Previous studies observed the change of interendothelial junction with the interaction of cavitating bubbles with endothelial cells. For example, vessel distention of 2.3 μm and invagination of 1.1 μm were observed during the expansion and contraction of the microbubbles on the milliseconds scale [29]. A similar model but at much higher pressure (~7.2 MPa) was used to observe vessel distention up to 10 μm and invagination up to 25 μm [102–104]. These studies demonstrate that the expanded phase of large bubbles causes a circumferential displacement of the vessels on a millisecond scale, thereby increasing dilatational strain and creating large gaps between cells, and that invagination of blood vessels occurs in the contraction phase of the bubble, leading to the delamination of the endothelial layer. The gaps between endothelial cells was found to require several minutes to form and remained for at least ten minutes under microbubbles oscillation, suggesting a prolonged, enhanced vascular permeability for macromolecular delivery [23].

Many studies found ultrasound-driven microbubbles could open blood-brain barrier (BBB), providing a time-window for macromolecular delivery [105]. These results demonstrated the transient nature of cavitation-induced junction opening and subsequent recovery [106]. For example, 40 kDa horseradish peroxidase and 139 Da lanthanum chloride molecules were observed to pass through BBB at 1 or 2 h after microbubbles were exposed to 1.5 MHz ultrasound with 1.1 MPa PNP and 1 Hz pulse repetition frequency (PRF) for 30 s, and then these tracers were absent after 4 h [107]. Park et al. used contrast-enhanced magnetic resonance imaging to track the kinetics of BBB permeability, and found that delivery efficacy across BBB decreased exponentially as a function of time with an estimated half-life of 2.22 h after microbubble were exposed to 690 kHz ultrasound with 10 ms pulse width, 1 Hz PRF and 0.8–1.1 MPa pressure for 60 s [106]. Using the same acoustic parameters, they also found the leakage of Magnevist across blood-retinal barrier up to 3.5 h [108]. Moreover, focused ultrasound-induced BBB opening was also reported to close within 24 h in rabbits, mice and monkeys [109–111]. All of these results indicate the duration of vascular permeability on the orders of hours.

The kinetics and magnitude of interendothelial junction opening and restoration are likely to be dependent on the type and dose of cavitation, as well as the location of the endothelial cells relative to the bubbles [105]. However, in contrast to the kinetics of membrane perforation and resealing, there is a lack of understanding of the spatiotemporal relationship between cavitation activities and the kinetics of the interendothelial junction. Tracking the dynamics of opening and recovery of the interendothelial junction is particularly challenging because of a lack of adequate technology to detect the dynamics and microscopic events of microbubble activities and the biological response in the vasculature.

3.2. Bioeffects in cavitation-opened interendothelial junctions

1) *Intracellular calcium activity*. Intracellular Ca^{2+} affects cell–cell contact, migration of tight junctions (TJs) protein Zona occluden-1 (ZO-1) from intracellular sites to the plasma membrane, and TJs assembly in endothelial and epithelial cells [112,113]. The increase in intracellular Ca^{2+} interferes with TJs formation while the decrease in intracellular Ca^{2+} alters ZO-1/actin binding and the subcellular localization of occludin [114]. Early studies indicated that intracellular Ca^{2+} fluctuation was involved in interendothelial TJs opening and BBB permeability increase [115,116]. More recently, it was revealed that Ca^{2+} influx in brain microvascular endothelial

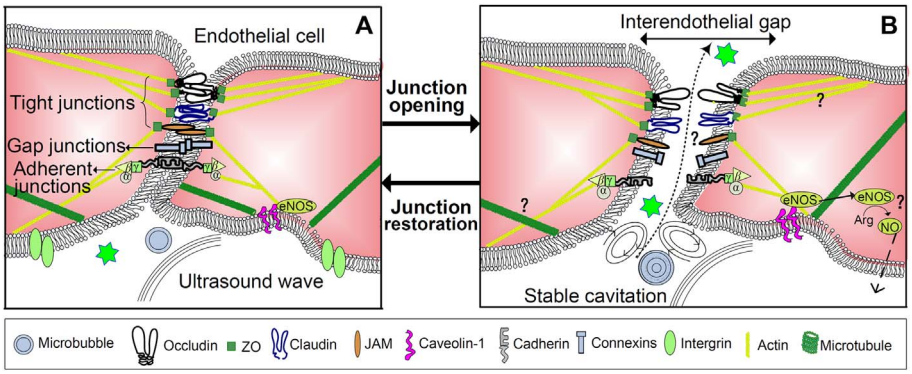

Fig. 4. Overview of the underlying mechanisms for the opening and restoration of intercellular junctions by the oscillating microbubbles. (A) Structural organization of interendothelial junction pre-exposure, including tight junctions (Occludin, claudin and junctional adhesion molecules (JAMs), adherens junctions (vascular endothelial (VE) cadherin) and gap junctions (Connexins). (B) Shear stress from oscillating microbubble results in the formation of interendothelial gap. Changes in the tight junctions, adherens junctions and gap junctions may be involved. Caveolin-1 detached from endothelial nitric oxide synthase (eNOS) converts arginine to nitric oxide, causing paracellular permeability. Changes in the cytoskeleton may disaggregate the proteins of the interendothelial junction.

cells exposed to ultrasound and microbubbles initially rose and then rapidly recovered [117]. This response is similar to that in sonoporated cells. Delayed Ca^{2+} influx in non-sonoporated cells suggests that a secondary messenger travels through the intercellular junction from one cell to another, and implies the role of Ca^{2+} influx in the interendothelial gap formation [19]. However, the downstream targets of Ca^{2+} influx and the causal relationship between intracellular Ca^{2+} and the interendothelial gap need to be further investigated.

2) *Temporal changes of interendothelial junction proteins*. Electron microscopy and immune-electron microscopy were used to analyze the molecular changes associated with cavitation-opened interendothelial junctions. Sheikov et al. found that the expression of trans-membrane protein Claudins (Claudin-1, Claudin-5) and ZO-1 significantly decreased 1–2 h after exposure to ultrasound and microbubbles. The protein levels increased after 4–6 h, then returned to normal levels after 24 h[107,118]. These temporal molecular changes indicate the gradual disintegration and reassembling of tight junction complexes post-exposure and also prove the transient nature of the interendothelial gap. Deng et al. observed a significant increase in the expression of caveolin-1 by western blot analysis 1 h after BBB exposed to ultrasound and microbubbles, suggesting that transcytosis is involved in the junction opening of the BBB [119]. However, as these studies rarely provide available information on cavitation events, it is difficult to quantitatively establish the relationship between cavitation activities and molecular changes of the interendothelial junctions. Moreover, because of the complexity of the interendothelial junction proteins, more sophisticated experiments need to be designed to investigate which molecular events are involved in the opening of the interendothelial junction and the spatiotemporal relationship between them.

3.3. Mechanisms of cavitation-opened interendothelial junctions

Endothelial cells maintain their flattened shape through centrifugal tension from the interconnection of focal adhesions, microtubules and interendothelial junctions that resist the centripetal tension from actin–myosin cross-bridging [120], as indicated in Figs. 4A or 5A. Under cavitation exposure, the interaction of shear stress from oscillating bubbles with the centripetal and centrifugal forces from endothelial cells may influence the cytoskeleton, interendothelial junctions and focal adhesion, resulting in increased interendothelial permeability, as shown in Fig. 4B. Moreover, the inertial collapse of microbubbles spontaneously induces membrane perforation accompanied by the contraction and shrinkage of cells, forming interendothelial gaps, as shown in Fig. 5B. Thus, changes in cell morphology may explain the cavitation-enhanced interendothelial permeability. However, during and after exposure to cavitation, it is necessary to investigate: (i) the spatiotemporal relationship between cavitating bubbles and the centripetal and centrifugal forces on endothelial cells, and (ii) which cellular and molecular responses contribute to increased interendothelial permeability and the mechanisms by which this occurs. The underlying mechanisms by which interendothelial permeability is increased through the oscillation and collapse of bubbles are listed below.

1) *Role of actin–myosin polymerization*. Stress fibers composed of bundles of polymerized actin and myosin filaments are the primary elements of the contractile apparatus of endothelial cells and influence the endothelial permeability [120,121]. Owing to the complexity of the linkages of actin with TJs, adheren junctions (AJs) and focal adhesions, actin polymerization influences the functions of TJs and AJs at specific sites, thereby affecting localized endothelial permeability [122]. Moreover, myosin light chain kinase (MLCK), phosphoprotein phosphatases (e.g. Okadaic acid, Calyculin), transient receptor channels, monomeric GTPase (e.g. RhoA, Rac, Cdc42) and actin polymerizing proteins (e.g. filamin, cortactin, gelsolin and cofilin) play important roles in actin-myosin-generated contraction. However, because of the non-uniform distribution of cavitation events around endothelial cells in a blood-flow environment, it is difficult to observe the spatiotemporal relationship between cavitation events and actin polymerization in real-time. Great efforts are needed to investigate how these factors above function in cavitation-opened interendothelial junctions and which proteins are sensitive to cavitation activities.

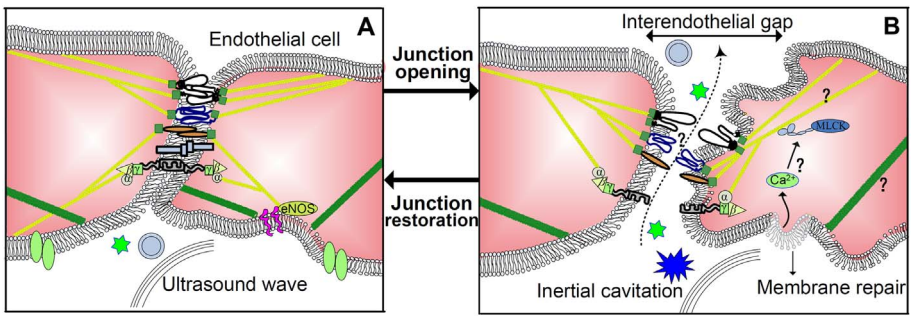

Fig. 5. Overview of the underlying mechanisms for the opening and restoration of intercellular junctions by the collapsing microbubbles. (A) Structural organization of interendothelial junction pre-exposure. All symbols illustrated in Fig. 4. (B) Collapsing microbubbles cause the formation of the interendothelial gap. Rapid contraction and deformation in sonoporated cells result in the changes of the cytoskeleton. The inverse relationship between actin and microtubules may weaken the junction proteins, thereby leading to paracellular gap. Ca^{2+}- dependent myosin light chain kinase (MLCK) possibly cause endothelial cell contraction and the resulting interendothelial gap.

2) *Role of interendothelial junction complexes*. Interendothelial junctions, composed of AJs (cadherin–catenin complexes) and TJs (occludin–claudin–ZO complexes), are stabilized by linkages to cortical actin filaments [123,124]. The reorganization of actin filaments into stress fibers results in the transmission of the contractile force to interendothelial junctions, thereby influencing intercellular junctions [125]. The expression levels of TJs and AJs protein complexes, which are regulated by RhoGTPase and phosphorylation, affect their ability to interact with each other or the actin filaments, leading to paracellular gaps [126]. Although the results described in Section 3.2 showed the expression levels of these proteins correlated with a change of interendothelial permeability post exposure, it remains unclear which biophysical signals trigger changes of these proteins during cavitation, and how these proteins interacts with each other.
3) *Role of microtubules and nitric oxide*. Although microtubules do not directly contact interendothelial junctions and focal adhesion complexes, they play a role in resisting the compression of cells by opposing actin–myosin contractility. Previous studies determined that depolymerization of microtubules regulated the state of actin polymerization and activated RhoA signaling, leading to interendothelial gap [127–129]. Therefore, the inverse relationship between the stability of actin stress fibers and microtubules is an important factor for weakening interendothelial junctions [127,128]. In addition, microtubules also influence endothelial permeability by regulating vesicular trafficking of adheren junction proteins to the junctions and focal adhesions. However, it remains unknown that how the microtubules function in the cavitation-enhanced interendothelia permeability.

   Nitric oxide is a potent vasodilator that regulates interendothelial contact [8,14]. Ca^{2+} influx or high shear stress from oscillating bubbles may liberate endothelial nitric oxide synthase (eNOS), which commonly binds with caveolin-1, a protein abundant within plasma membrane clefts. Subsequently, liberated eNOS converts arginine into nitric oxide, thereby regulating the intercellular junctions [130,131]. Moreover, some mechanoreceptors on the membrane surface may be activated by the increased shear stress, resulting in the caveolin-1 opening the interendothelial junctions.

3.4. Mechanism of restoration of cavitation-opened interendothelial junctions

The gradual restoration of the interendothelial integrity, which counters the effect of increasing endothelial permeability, raises another important issue in terms of biosafety and efficacy [3,105]. In contrast to the formation of interendothelial gaps, which is dependent on the interaction between microbubbles and cells, interendothelial junction restoration is an active biological process that involves a variety of biochemical events.

Cdc42 and Rac, which are known as filament-binding partners, have been shown to regulate the formation and organization of actin filaments associated with membrane ruffles, filopodia and lamellipodia in endothelial cells [132,133]. Cdc42 activation regulates AJs disassembly as well as reassembly to modulate interendothelial junctions. Rac function is required to maintain a normal interendothelial barrier and decreased Rac activity enhances interendothelial permeability [122,134]. Recent studies indicated that the expression and inhibition of focal adhesion kinase maintained endothelial barrier integrity and irreversibly increased the permeability of the endothelial barrier, respectively [135,136]. In addition, activation and inhibition of RhoA can also disassemble AJs and restore interendothelial junctions, respectively [137,138]. Therefore, focal adhesion kinase-induced down modulation of RhoA activity is crucial for restoration of endothelial barrier integrity [139–141]. Cyclic adenosine monophosphate (cAMP) activation can strengthen the endothelial barrier by activating cAMP-dependent protein kinase A, which mainly inhibits endothelial contraction by preventing the activation of RhoA and MLCK, and increases barrier function by binding to occludin and ZO-1 [142,143]. However, almost no studies have investigated how these regulatory networks function during the restoration of cavitation-opened interendothelial junctions. A deeper understanding of the mechanism of interendothelial junction restoration may help modulate the duration of interendothelial junction opening and design an optimized time window for improving the kinetics of macromolecular delivery into the targeted region.

4. Endocytosis stimulated by acoustic cavitation

Compared with the passive diffusion of macromolecules into the cytosol and extravascular tissue as a result of sonoporation and cavitation-opened interendothelial junctions, respectively, cavitation-stimulated endocytosis — an active delivery route by which macromolecules are taken up into cells — is considered to be a potentially safe pathway for drug delivery. To regulate cavitation-stimulated endocytosis, it is important to determine when and how endocytosis occurs post-cavitation and how long it continues.

4.1. Spatiotemporal characteristics of cavitation-induced endocytosis

Recent studies provided preliminarily spatiotemporal information on endocytosis activity by detecting endocytotic markers at different time-points post-exposure. The macromolecular delivery efficacy was found to continuously increase for 4 h after microbubbles exposed to ultrasound at 0.15–0.2 MPa PNP. Using real-time fluorescence imaging, SYTOX Green was observed to be internalized for several hours from 52 s after 0.2 MPa PNP ultrasound exposure to microbubbles. Moreover, inhibition of endocytosis pathways caused a substantial increase in the time of the occurrence of uptake post-exposure [144]. For example, fluorescent markers, such as transferrin and Lucifer yellow, which are indicative of receptor and fluid phase endocytosis, respectively, were observed to markedly increase 30 min after exposure to 0.1 MPa PNP ultrasound [25]. Another endocytotic marker, clathrin, was observed to immediately accumulate in the cytoplasm, and substantially reduce in concentration 18 h after exposure to 30 min of 0.2 MPa PNP ultrasound alone [145]. Similar results also found that clathrin mediated-endocytosis was enhanced through the assembly of clathrin-coated pits within about 5 min after exposure to ultrasound and microbubbles [146]. These findings indicate that endocytosis occurs at a relatively delayed time-point (several minutes post-exposure) and lasts for a long period.

In contrast to homogeneous distribution of small molecules (4.4–70 kDa) throughout the whole cytosol after sonoporation, macromolecules (155–500 kDa) internalized by endocytosis exhibited vesicle-like structures that were randomly distributed throughout the cytosol [24]. A large number of uncoated pits representative of endocytosis were found to scatter on the surface of the cell membrane via SEM [31]. Because endocytosis is determined by active cellular behaviors, it is difficult to explore the spatial relationship between endocytosis and cavitation events.

4.2. Bioeffects in cavitation-stimulated endocytosis

1) *Intracellular calcium transient*. Meijering et al. demonstrated that intracellular calcium simultaneously increased and reached a peak at about 30 s post-exposure, and then gradually restored to the normal level in the following 30 s [24]. Ca^{2+} influx from the extracellular environment through transient membrane perforation could act as an effector for triggering endocytosis. Maria reported that calcium influx began 45 s post-exposure, and could improve the transfection rates of plasmid DNA by endocytosis [147]. Other studies have indicated that a high concentration of intracellular Ca^{2+} played a crucial role in the clathrin-mediated endocytosis pathway,

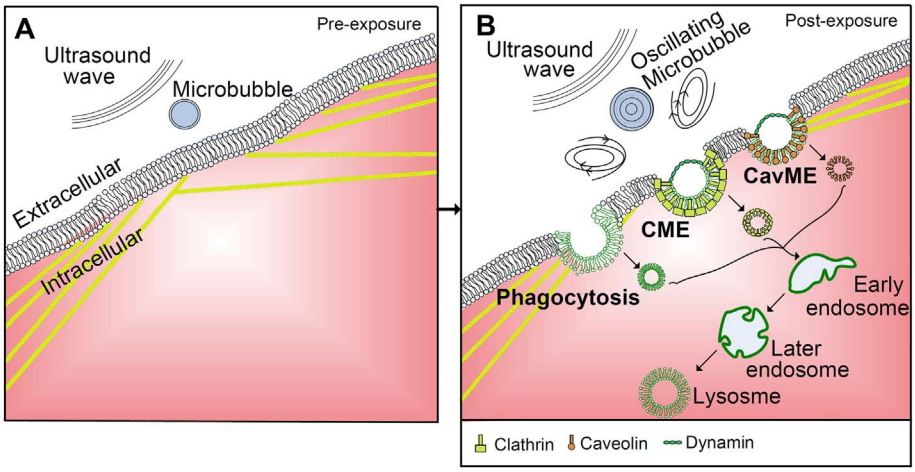

Fig. 6. Overview of the mechanisms of endocytosis enhancement by stable cavitation. (A) A cell with a lipid bilayer underlying actin and intracellular vesicles pre-exposure. (B) Several pathways, including phagocytosis, Clathrin-mediated endocytosis (CME) and caveolin-mediated endocytosis (CavME), may be triggered by the oscillating microbubbles. CME and CavME occur through clathrin-coated pits and caveolae, respectively. The internalized vesicles undergo homotypic fusion to form early endosomes, which could be trafficked through late endosome to the lysosome for degradation.

and also had a strong influence on the cytoskeleton components in the cells' cortex [25]. However, how the intracellular calcium transients activates endocytosis remains unclear.

2) *Production of reactive oxygen species*. Pulsed ultrasound has been shown to trigger intracellular oxidative stress in a time- and dose-dependent manner [148]. ROS production was found to increase soon after the onset of ultrasound exposure and continue for a long period after cessation of the ultrasound. Moreover, ROS production exhibited longer lasting and reached higher concentrations after exposure to higher ultrasound intensities [147]. The presence of antioxidants could significantly reduce the delivery efficiency via ultrasound-induced endocytosis, which suggests that endocytosis may be activated by a ROS-dependent mechanism, such as internalization of caveolae owing to ROS-induced caveolin-1 phosphorylation [149]. The ROS level may also have a direct effect on calcium influx, and thus causing endocytosis activity [24]. Yet these findings do not provide a detailed mechanism of the origin and role of ROS in cavitation-stimulated endocytosis.
3) *Lysosome exocytosis*. Lysosome exocytosis occurs upon membrane damage and plays an important role in the enhancement of endocytosis [93,96,150]. Lysosomal marker protein Lamp-1 was observed to accumulate at the plasma membrane, which suggests that lysosome exocytosis occurs at the same time as endocytosis induced by ultrasound in the presence of microbubbles [146]. Vacuolin-1 and desipramine, which inhibit lysosome exocytosis and acid sphingomyelinase, respectively, were found to reduce the activity of the cell surface transferrin receptor, suggesting that lysosome exocytosis contributes to the regulation of calthrin-dependent endocytosis induced by cavitation [146]. Dec Coke et al. observed the co-localization of internalized macromolecules by endocytic uptake and lysosomes, suggesting that lysosomes are involved in cavitation-stimulated endocytosis [30].

4.3. Mechanism of endocytosis induced by cavitation

The underlying mechanism responsible for cavitation-induced endocytosis has not been clearly elucidated. Some of the possible biophysical events involved in this process are shown in Fig. 6.

4.3.1. Main biophysical mechanisms

Endocytosis is initiated by upstream physical (caused by the interaction between microbubbles and ultrasound) or biological signals (triggered by physical signals or sonoporation) after exposure to ultrasound in the presence of microbubbles.

1) *Physical signals for inducing endocytosis*. Membrane deformation, which is thought to play a role in endocytosis, may be elicited by several physical signals, as described below. The primary radiation force from the acoustic pressure pushes bubbles in the direction of ultrasound propagation and compresses them onto the plasma membrane, leading to membrane deformation and indentation [151,152]. Secondary radiation forces between bubbles cause microbubble aggregation and contribute to membrane deformation [153,154]. Importantly, oscillating bubbles exerted shear stress on the membrane, resulting in membrane deformation [52]. Shear stress is known to induce endocytic activity in endothelial cells [14,99]. However, direct, conclusive evidence for a relationship between these physical signals and endocytosis is lacking.
2) *Conversion of physical to biochemical signals*. External mechanical forces can be transmitted along the cytoskeleton, causing spatial changes in cytoskeletal-associated proteins and enzymes related to signal transduction (i.e. kinases) [155]. Moreover, extracellular physical forces can be converted into biochemical reactions, such as ROS production [155]. It is well established that the interaction of ultrasound with microbubbles elicits the deformation and remodeling of the cytoskeleton [156,157].Subsequently, some mechano-sensors (e.g. integrins, stretch-activated ion channels) sense these changes, transducing the mechanical signal to activate endocytosis and exocytosis, thereby normalizing the membrane tension [158–160]. The deformation of cytoskeleton also could enhance caveolar membrane trafficking [161]. However, further investigation is needed to identify the biochemical signals related to the cytoskeleton and to determine how they spatiotemporally relate to endocytosis post-cavitation.
3) *Endocytosis related to sonoporation*. Mechanically perforated membranes may be responsible for endocytosis. On the one hand, endocytosis is directly activated and physically reseals small membrane perforations, which are generally caused by the oscillating microbubbles [19,95]. One the other hand, pre-formation of lysosomal patches and exocytosis is required for resealing large membrane pores, which are mainly elicited by the collapsing microbubbles [94,162]. Lysosomal acid sphingomyelinase released by exocytosis converts sphingomyeline in the cell membrane to ceramide, promoting inward budding and vesicle formation [163,164]. This serves as a prelude to the activation of endocytosis. Moreover, other bioeffects associated with sonoporation also contribute to the enhancement of endocytosis [42,165]. For example, under Ca^{2+} influx, membrane domains rich in cholesterol can spontaneously vesiculate and form endocytic vesicles [166].

4.3.2. Endocytic pathways

In general, two main endocytic pathways are involved in endocytosis: clathrin-dependent (receptor-mediated endocytosis) and clathrin-independent (caveolin-mediated endocytosis) [167]. The

inhibition of clathrin-dependent endocytosis substantially affected the internalization of macromolecules (600-Da and 4.4–500 kDa), whereas the inhibition of caveolin-mediated endocytosis only had effect on the delivery of larger molecules (155–500 kDa) [24]. These findings support a link between the macromolecule size and its route of cellular entry. The inhibition of the caveolin-mediated endocytosis pathway with genistein decreased the number of the uncoated pits after exposure to ultrasound and bubbles, thus confirming that sonoporation stimulates caveolin-dependent endocytosis [31]. Similar results found that high intensity ultrasound increased endothelial permeability through the selective enhancement of caveolin-dependent endocytosis while leaving clathrin-dependent endocytosis unaltered [149]. Conversely, a recent real-time study found a larger increase in uptake time constants when the clathrin-mediated pathway was inhibited than when the caveolin-mediated pathway was inhibited after cavitation treatment [144]. Similarly, delivery efficacy was greatly inhibited after blocking clathrin-mediated endocytosis pathway using chlorpromazine, but no significant change was found after inhibiting the caveolin-mediated pathway using filipin III or genistein [168]. These seemingly contradictory results raise the question of what factors other than molecular size determine the preferred route of cellular entry under the influence of ultrasound-driven microbubbles. Rigorous investigations are required to further clarify these problems.

5. Challenges, perspectives and conclusions

5.1. Challenges

1) *Achieving uniform and controllable bioeffects*. It is expected that the targeted cells or tissues will be subjected to uniform and homogenous cavitation exposure, thereby achieving uniform and even controllable bioeffects that is crucial to achieve satisfactory efficacy and safety. However, microbubbles are the discrete entities with different sizes distributed in the blood and confined within the vasculature, resulting in non-uniform cavitation activities around the limited cells. Consequently, it is a challenging task to achieve uniform cavitation behavior and bioeffects in the targeted region.
   The novel microbubbles, that are specifically tailored and designed for ultrasonic response, load and penetration capacity, may be more desired and necessary to solve this problem. For example, monodisperse microbubbles would allow for relatively uniform cavitation to be caused by minimal ultrasound energy at specific frequency, thereby minimizing adverse effects caused by non-uniform and excessive ultrasound energy [169]. Emerging nanobubbles have the potential to diffuse from vasculature into the targeted tissues, possibly increasing the penetration depth of drug [43,170]. On the other side, it is essential to spatially and temporally monitor and control cavitation activities in vivo. Passive cavitation mapping and feedback control strategies has been developed to monitor and control the spatiotemporal distribution of cavitation activities [171–173]. It is also expected that these promising technologies will be implemented in applications.
2) *Identifying the bioeffects in cavitation-enhanced permeability*. Various physical, biophysical, biological and even biochemical processes in different spatial and temporal scales are involved in the interaction of ultrasound-driven microbubbles with the cells and tissues. Such complex factors pose a big challenge to identify the bioeffects and the related biological mechanisms associated with cavitation-enhanced permeability. In addition, due to the variability of acoustic pressure in situ and the complexity of the local cellular microenvironments, it is difficult to directly relate the specific cavitation activity to the resulting bioeffects. Moreover, whether the identified bioeffects and regulatory mechanisms by in vitro experiments are consistent with those that occur in vivo also needs to be further determined.

5.2. Future perspectives

1) *Establishing a standardized research methodology*. Due to the complexity of the cavitation activities and the resulting bioeffects, for future in vitro and ex vivo studies, establishing a systematic and rigorous live-cell platform, characterized by real-time monitoring cavitation events in the targeted region, fast recording of the cellular and even molecular responses during and after cavitation treatment, will facilitate understanding of the spatiotemporal bioeffects that contribute to cavitation-enhanced delivery. More importantly, using such a methodology would simplify the comparison of results from different studies and boost progress in the applications of this approach. For future studies in vivo and therapeutic applications, developing a novel imaging approach that can provide anatomical guidance pre-exposure, monitor the cavitation activities and cellular responses and trace the kinetics of the delivery during exposure, and evaluate drug distribution and physiological status post-exposure, will be of great value for precise, effective and safe delivery.
2) *Designing biological strategies to regulate cavitation-enhanced delivery*. Mechanistic understanding the bioeffects in cavitation-enhanced delivery will lead to the design of biology-based strategies to regulate the time window of permeability enhancement and thus improve the efficacy and biosafety.
   With regard to sonoporation, it is important to identify the determinative factors for the membrane resealing, as well as the early and late biochemical signals related to the fate of the sonoporated cells. The intracellular Ca^{2+} level has been identified as a double-edged sword in regulating the kinetics of sonoporation and the fate of sonoporated cells, in that it acts not only as an initiator for membrane resealing by endocytosis or exocytosis, but also as toxic for triggering apoptosis. Therefore, intervention in Ca^{2+}-related pathways using biochemical methods could assist in improving the efficacy and safety of sonoporation-based delivery. For example, intracellular Ca^{2+} chelators could inhibit the mitochondria-caspase apoptotic pathway, thus reducing DNA fragmentation in the sonoporated cells. A stabilizer for actin filaments might be used to facilitate membrane resealing or to inhibit apoptosis and necrosis.
   To regulate cavitation-induced interendothelial gap and subsequently restoration, it is important to identify crucial regulatory factors that take place during and after the interaction of cavitation with endothelial cells. For example, intervention in core proteins (e.g. Cdc42, Rac) might regulate restoration of intercellular junctions and thus provide an optimal window for delivery. In addition, because of the important role of actin-myosin in interendothelial gap formation, adding an agent that polymerizes actin filaments pre-exposure might promote the fast opening of intercellular junctions, thereby improving delivery efficacy. For cavitation-stimulated endocytosis, which kind of endocytic pathways and what molecular mechanisms are mainly recruited by oscillating bubbles for different cell types need to be determined. Such identified pathways related to the endocytosis may lead to the design of novel strategies for enhancing cavitation-stimulated endocytosis.

5.3. Conclusions

Promising progress has been made in understanding the bioeffects involved in cavitation-enhanced macromolecule delivery. However, we still lack detailed knowledge on the cellular and molecular responses associated with sonoporation, cavitation-induced interendothelial gap and endocytosis. Therefore, mechanistic understanding the bioeffects involved in cavitation-enhanced permeability need to be extended to consolidate the current knowledge base. It is also important to investigate these fundamental scientific issues behind this approach, which could ensure the rational, efficient and safe execution of this approach, and promote the translation into therapeutic applications.

Acknowledgements

This research is funded by the National Natural Science Foundation of China (Nos. 81471667, 31630007), Program of Medicine and Engineering Cross Fund of Shanghai Jiao Tong University (YG2015ZD09), SMC Rising Star Fund of Shanghai Jiao Tong University (16X100080028).

References

[1] A.L.K.S. Hernot, Microbubbles in ultrasound-triggered drug and gene delivery, Adv. Drug Deliv. Rev. 60 (2008) 1153–1166.
[2] W. Tzu-Yin, K.E. Wilson, S. Machtaler, J.K. Willmann, Ultrasound and microbubble guided drug delivery: mechanistic understanding and clinical implications, Curr. Pharm. Biotechnol. 14 (2013) 743–752.
[3] C.X. Deng, Targeted drug delivery across the blood-brain barrier using ultrasound technique, Ther. Deliv. 1 (2010) 819–848.
[4] A.T. Lefor, S. Makohon, N.B. Ackerman, The effects of hyperthermia on vascular permeability in experimental liver metastasis, J. Surg. Oncol. 28 (1985) 297–300.
[5] G. Kong, R.D. Braun, M.W. Dewhirst, Characterization of the effect of hyperthermia on nanoparticle extravasation from tumor vasculature, Cancer Res. 61 (2001) 3027–3032.
[6] C.C. Coussios, C.H. Farny, G.T. Haar, R.A. Roy, Role of acoustic cavitation in the delivery and monitoring of cancer treatment by high-intensity focused ultrasound (HIFU), Int. J. Hyperth. 23 (2007) 105–120.
[7] V.A. Khokhlova, M.R. Bailey, J.A. Reed, B.W. Cunitz, P.J. Kaczkowski, L.A. Crum, Effects of nonlinear propagation, cavitation, and boiling in lesion formation by high intensity focused ultrasound in a gel phantom, J. Acoust. Soc. Am. 119 (2006) 1834–1848.
[8] J. Wu, Shear stress in cells generated by ultrasound, Prog. Biophys. Mol. Biol. 93 (2007) 363–373.
[9] R. Lencioni, Enhancing the Role of Ultrasound with Contrast Agents, Springer-Verlag, Italia, 2006, pp. 1–23.
[10] A.L. Klibanov, Ultrasound contrast agents: development of the field and current status, Top. Curr. Chem. 222 (2002) 73–106.
[11] T. Faez, M. Emmer, K. Kooiman, M. Versluis, A.F.W. van der Steen, N. de Jong, 20 years of ultrasound contrast agent modeling, IEEE Trans. Ultrason. Ferroelectr. Freq. Control 60 (2013) 7–20.
[12] K. Ferrara, R. Pollard, M. Borden, Ultrasound microbubble contrast agents: fundamentals and application to gene and drug delivery, Annu. Rev. Biomed. Eng. 9 (2007) 415–447.
[13] V. Sboros, Response of contrast agents to ultrasound, Adv. Drug Deliv. Rev. 60 (2008) 1117–1136.
[14] E. VanBavel, Effects of shear stress on endothelial cells: possible relevance for ultrasound applications, Prog. Biophys. Mol. Biol. 93 (2007) 374–383.
[15] J. Collis, R. Manasseh, P. Liovic, P. Tho, A. Ooi, K. Petkovic-Duran, Y. Zhu, Cavitation microstreaming and stress fields created by microbubbles, Ultrasonics 50 (2010) 273–279.
[16] T. Kodama, Y. Tomita, Cavitation bubble behavior and bubble-shock wave interaction near a gelatin surface as a study of in vivo bubble dynamics, Appl. Phys. B Lasers Opt. 70 (2000) 139–149.
[17] M. Postema, A. van Wamel, F.J. ten Cate, N. de Jong, High-speed photography during ultrasound illustrates potential therapeutic applications of microbubbles, Med. Phys. 32 (2005) 3707–3711.
[18] F. Yuan, C. Yang, P. Zhong, Cell membrane deformation and bioeffects produced by tandem bubble-induced jetting flow, Proc. Natl. Acad. Sci. U. S. A. 112 (2015) E7039–E7047.
[19] I. Lentacker, I. De Cock, R. Deckers, S.C. De Smedt, C.T. Moonen, Understanding ultrasound induced sonoporation: definitions and underlying mechanisms, Adv. Drug Deliv. Rev. 72 (2014) 49–64.
[20] A. van Wamel, K. Kooiman, M. Harteveld, M. Emmer, F.J. ten Cate, M. Versluis, N. de Jong, Vibrating microbubbles poking individual cells: drug transfer into cells via sonoporation, J. Control. Release 112 (2006) 149–155.
[21] Y. Hu, J.M. Wan, A.C. Yu, Membrane perforation and recovery dynamics in microbubble-mediated sonoporation, Ultrasound Med. Biol. 39 (2013) 2393–2405.
[22] K. Hynynen, Ultrasound for drug and gene delivery to the brain, Adv. Drug Deliv. Rev. 60 (2008) 1209–1217.
[23] B. Helfield, X.C. Chen, S.C. Watkins, F.S. Villanueva, Biophysical insight into mechanisms of sonoporation, Proc. Natl. Acad. Sci. U. S. A. 113 (2016) 9983–9988.
[24] B.D.M. Meijering, L.J.M. Juffermans, A. van Wamel, R.H. Henning, I.S. Zuhorn, M. Emmer, A.M.G. Versteilen, W.J. Paulus, W.H. van Gilst, K. Kooiman, N. de Jong, R.J.P. Musters, L.E. Deelman, O. Kamp, Ultrasound and microbubble-targeted delivery of macromolecules is regulated by induction of endocytosis and pore formation, Circ. Res. 104 (2009) (679-U226).
[25] J. Hauser, M. Ellisman, H.U. Steinau, E. Stefan, M. Dudda, M. Hauser, Ultrasound enhanced endocytotic activity of human fibroblasts, Ultrasound Med. Biol. 35 (2009) 2084–2092.
[26] S.R. Sirsi, M.A. Borden, Advances in ultrasound mediated gene therapy using microbubble contrast agents, Theranostics 2 (2012) 1208–1222.
[27] G.A. Husseini, W.G. Pitt, Micelles and nanoparticles for ultrasonic drug and gene delivery, Adv. Drug Deliv. Rev. 60 (2008) 1137–1152.
[28] Z. Fan, H. Liu, M. Mayer, C.X. Deng, Spatiotemporally controlled single cell sonoporation, Proc. Natl. Acad. Sci. U. S. A. 109 (2012) 16486–16491.
[29] C.F. Caskey, S.M. Stieger, S. Qin, P.A. Dayton, K.W. Ferrara, Direct observations of ultrasound microbubble contrast agent interaction with the microvessel wall, J. Acoust. Soc. Am. 122 (2007) 1191–1200.
[30] I. De Cock, E. Zagato, K. Braeckmans, Y. Luan, N. de Jong, S.C. De Smedt, I. Lentacker, Ultrasound and microbubble mediated drug delivery: acoustic pressure as determinant for uptake via membrane pores or endocytosis, J. Control. Release 197 (2015) 20–28.
[31] A. Zeghimi, J.M. Escoffre, A. Bouakaz, Role of endocytosis in sonoporation-mediated membrane permeabilization and uptake of small molecules: a electron microscopy study, Phys. Biol. 12 (2015).
[32] A. Xie, T. Belcik, Y. Qi, T.K. Morgan, S.A. Champaneri, S. Taylor, B.P. Davidson, Y. Zhao, A.L. Klibanov, M.A. Kuliszewski, H. Leong-Poi, A. Ammi, J.R. Lindner, Ultrasound-mediated vascular gene transfection by cavitation of endothelial-targeted cationic microbubbles, JACC Cardiovasc. Imaging 5 (2012) 1253–1262.
[33] L.H. Treat, N. McDannold, N. Vykhodtseva, Y.Z. Zhang, K. Tam, K. Hynynen, Targeted delivery of doxorubicin to the rat brain at therapeutic levels using MRI-guided focused ultrasound, Int. J. Cancer 121 (2007) 901–907.
[34] M. Kinoshita, N. McDannold, F.A. Jolesz, K. Hynynen, Noninvasive localized delivery of Herceptin to the mouse brain by MRI-guided focused ultrasound-induced blood-brain barrier disruption, Proc. Natl. Acad. Sci. U. S. A. 103 (2006) 11719–11723.
[35] R. Bekeredjian, P.A. Grayburn, R.V. Shohet, Use of ultrasound contrast agents for gene or drug delivery in cardiovascular medicine, J. Am. Coll. Cardiol. 45 (2005) 329–335.
[36] S.T. Laing, H. Kim, J.A. Kopechek, D. Parikh, S.L. Huang, M.E. Klegerman, C.K. Holland, D.D. McPherson, Ultrasound-mediated delivery of echogenic immunoliposomes to porcine vascular smooth muscle cells in vivo, J. Liposome Res. 20 (2010) 160–167.
[37] R. Suzuki, E. Namai, Y. Oda, N. Nishiie, S. Otake, R. Koshima, K. Hirata, Y. Taira, N. Utoguchi, Y. Negishi, S. Nakagawa, K. Maruyama, Cancer gene therapy by IL-12 gene delivery using liposomal bubbles and tumoral ultrasound exposure, J. Control. Release 142 (2010) 245–250.
[38] K. Yamaguchi, L.B. Feril, K. Tachibana, A. Takahashi, M. Matsuo, H. Endo, Y. Harada, J. Nakayama, Ultrasound-mediated interferon beta gene transfection inhibits growth of malignant melanoma, Biochem. Biophys. Res. Commun. 411 (2011) 137–142.
[39] P. Haag, F. Frauscher, J. Gradl, A. Seitz, G. Schafer, J.R. Lindner, A.L. Klibanov, G. Bartsch, H. Klocker, I.E. Eder, Microbubble-enhanced ultrasound to deliver an antisense oligodeoxynucleotide targeting the human androgen receptor into prostate tumours, J. Steroid Biochem. 102 (2006) 103–113.
[40] M.J.E. Kuijpers, K. Gilio, S. Reitsma, R. Nergiz-Unal, L. Prinzen, S. Heeneman, E. Lutgens, M.A.M.J. Zandvoort, B. Nieswandt, M.G.A.O. Egbrink, J.W.M. Heemskerk, Complementary roles of platelets and coagulation in thrombus formation on plaques acutely ruptured by targeted ultrasound treatment: a novel intravital model, J. Thromb. Haemost. 7 (2009) 152–161.
[41] N. Kobayashi, T. Yasu, S. Yamada, N. Kudo, M. Kuroki, M. Kawakami, K. Miyatake, M. Saito, Endothelial cell injury in venule and capillary induced by contrast ultrasonography, Ultrasound Med. Biol. 28 (2002) 949–956.
[42] M.A. Hassan, P. Campbell, T. Kondo, The role of Ca(2 +) in ultrasound-elicited bioeffects: progress, perspectives and prospects, Drug Discov. Today 15 (2010) 892–906.
[43] C. Hernandez, S. Gulati, G. Fioravanti, P.L. Stewart, A.A. Exner, Cryo-EM visualization of lipid and polymer-stabilized perfluorocarbon gas nanobubbles - a step towards nanobubble mediated drug delivery, Sci. Rep. 7 (2017).
[44] C.D. Arvanitis, M. Bazan-Peregrino, B. Rifai, L.W. Seymour, C.C. Coussios, Cavitation-enhanced extravasation for drug delivery, Ultrasound Med. Biol. 37 (2011) 1838–1852.
[45] D.M. Hallow, A.D. Mahajan, M.R. Prausnitz, Ultrasonically targeted delivery into endothelial and smooth muscle cells in ex vivo arteries, J. Control. Release 118 (2007) 285–293.
[46] K. Kooiman, H.J. Vos, M. Versluis, N. de Jong, Acoustic behavior of microbubbles and implications for drug delivery, Adv. Drug Deliv. Rev. 72 (2014) 28–48.
[47] H. Yu, L. Xu, Cell experimental studies on sonoporation: state of the art and remaining problems, J. Control. Release 174 (2014) 151–160.
[48] B. Geers, H. Dewitte, S.C. De Smedt, I. Lentacker, Crucial factors and emerging concepts in ultrasound-triggered drug delivery, J. Control. Release 164 (2012) 248–255.
[49] D.L. Miller, S.V. Pislaru, J.E. Greenleaf, Sonoporation: mechanical DNA delivery by ultrasonic cavitation, Somat. Cell Mol. Genet. 27 (2002) 115–134.
[50] K. Tachibana, T. Uchida, K. Ogawa, N. Yamashita, K. Tamura, Induction of cell-membrane porosity by ultrasound, Lancet 353 (1999) 1409.
[51] C.X. Deng, F. Sieling, H. Pan, J. Cui, Ultrasound-induced cell membrane porosity, Ultrasound Med. Biol. 30 (2004) 519–526.
[52] S.M. Nejad, S.H.R. Hosseini, H. Akiyama, K. Tachibana, Optical observation of cell sonoporation with low intensity ultrasound, Biochem. Biophys. Res. Commun. 413 (2011) 218–223.
[53] Z. Fan, D. Chen, C.X. Deng, Characterization of the dynamic activities of a population of microbubbles driven by pulsed ultrasound exposure in sonoporation, Ultrasound Med. Biol. 40 (2014) 1260–1272.
[54] N. Kudo, K. Okada, K. Yamamoto, Sonoporation by single-shot pulsed ultrasound with microbubbles adjacent to cells, Biophys. J. 96 (2009) 4866–4876.
[55] M. Ward, J. Wu, J.F. Chiu, Experimental study of the effects of Optison concentration on sonoporation in vitro, Ultrasound Med. Biol. 26 (2000) 1169–1175.
[56] S. Le Gac, E. Zwaan, A. van den Berg, C.D. Ohl, Sonoporation of suspension cells with a single cavitation bubble in a microfluidic confinement, Lab Chip 7 (2007)

1666–1672.
[57] Y. Zhou, K. Yang, J. Cui, J.Y. Ye, C.X. Deng, Controlled permeation of cell membrane by single bubble acoustic cavitation, J. Control. Release 157 (2012) 103–111.
[58] P. Qin, L. Xu, T. Han, L.F. Du, A.C.H. Yu, Effect of non-acoustic parameters on heterogeneous sonoporation mediated by single-pulse ultrasound and microbubbles, Ultrason. Sonochem. 31 (2016) 107–115.
[59] M.J. Shortencarier, P.A. Dayton, S.H. Bloch, P.A. Schumann, T.O. Matsunaga, K.W. Ferrara, A method for radiation-force localized drug delivery using gas-filled lipospheres, IEEE Trans. Ultrason. Ferroelectr. Freq. Control 51 (2004) 822–831.
[60] K. Kooiman, M. Foppen-Harteveld, A.F. van der Steen, N. de Jong, Sonoporation of endothelial cells by vibrating targeted microbubbles, J. Control. Release 154 (2011) 35–41.
[61] Y. Zhou, R.E. Kumon, J.M. Cui, C.X. Deng, The size of sonoporation pores on the cell membrane, Ultrasound Med. Biol. 35 (2009) 1756–1760.
[62] K. Okada, N. Kudo, K. Niwa, K. Yamamoto, A basic study on sonoporation with microbubbles exposed to pulsed ultrasound, J. Med. Ultrason. 32 (2005) 3–11.
[63] R. Karshafian, S. Samac, P.D. Bevan, P.N. Burns, Microbubble mediated sonoporation of cells in suspension: Clonogenic viability and influence of molecular size on uptake, Ultrasonics 50 (2010) 691–697.
[64] S. Mehier-Humbert, T. Bettinger, F. Yan, R.H. Guy, Plasma membrane poration induced by ultrasound exposure: implication for drug delivery, J. Control. Release 104 (2005) 213–222.
[65] Y. Qiu, Y. Luo, Y. Zhang, W. Cui, D. Zhang, J. Wu, J. Zhang, J. Tu, The correlation between acoustic cavitation and sonoporation involved in ultrasound-mediated DNA transfection with polyethylenimine (PEI) in vitro, J. Control. Release 145 (2010) 40–48.
[66] P. Prentice, A. Cuschierp, K. Dholakia, M. Prausnitz, P. Campbell, Membrane disruption by optically controlled microbubble cavitation, Nat. Phys. 1 (2005) 107–110.
[67] Z. Fan, D. Chen, C.X. Deng, Improving ultrasound gene transfection efficiency by controlling ultrasound excitation of microbubbles, J. Control. Release 170 (2013) 401–413.
[68] P. Qin, L. Xu, Y. Hu, W. Zhong, P. Cai, L. Du, L. Jin, A.C.H. Yu, Sonoporation-induced depolarization of plasma membrane potential: analysis of heterogeneous impact, Ultrasound Med. Biol. 40 (2014) 979–989.
[69] Z. Fan, R.E. Kumon, J. Park, C.X. Deng, Intracellular delivery and calcium transients generated in sonoporation facilitated by microbubbles, J. Control. Release 142 (2010) 31–39.
[70] R.E. Kumon, M. Aehle, D. Sabens, P. Parikh, Y.W. Han, D. Kourennyi, C.X. Deng, Spatiotemporal effects of sonoporation measured by real-time calcium imaging, Ultrasound Med. Biol. 35 (2009) 494–506.
[71] J. Park, Z. Fan, R.E. Kumon, M.E.H. El-Sayed, C.X. Deng, Modulation of intracellular Ca2 + concentration in brain microvascular endothelial cells in vitro by acoustic cavitation, Ultrasound Med. Biol. 36 (2010) 1176–1187.
[72] L.J.M. Juffermans, P.A. Dijkmans, R.J.P. Musters, C.A. Visser, O. Kamp, Transient permeabilization of cell membranes by ultrasound-exposed microbubbles is related to formation of hydrogen peroxide, Am. J. Physiol. Heart Circ. Physiol. 291 (2006) H1595–H1601.
[73] L.J. Juffermans, P.A. Dijkmans, R.J. Musters, O. Kamp, Formation of reactive oxygen species in the presence of ultrasound-exposed microbubbles is related to transient permeabilization of cell membranes, 78th Annual Scientific Session of the American-Heart-Association, Dallas, 2005, p. U697.
[74] H. Honda, T. Kondo, Q.L. Zhao, L.B. Feril Jr., H. Kitagawa, Role of intracellular calcium ions and reactive oxygen species in apoptosis induced by ultrasound, Ultrasound Med. Biol. 30 (2004) 683–692.
[75] S. Boitano, E.R. Dirksen, M.J. Sanderson, Intercellular propagation of calcium waves mediated by inositol trisphosphate, Science 258 (1992) 292–295.
[76] E.M. Schwiebert, Extracellular ATP-mediated propagation of Ca2 + waves. Focus on “Mechanical strain-induced Ca2 + waves are propagated via ATP release and purinergic receptor activation”, Am. J. Physiol. Cell Physiol. 279 (2000) C281–C283.
[77] H. Sauer, J. Hescheler, M. Wartenberg, Mechanical strain-induced Ca2 + waves are propagated via ATP release and purinergic receptor activation, Am. J. Physiol. Cell Physiol. 279 (2000) C295–C307.
[78] E.B. Babiychuk, K. Monastyrskaya, S. Potez, A. Draeger, Intracellular Ca2 + operates a switch between repair and lysis of streptolysin O-perforated cells, Cell Death Differ. 16 (2009) 1126–1134.
[79] T.A. Tran, J.Y. Le Guennec, P. Bougnoux, F. Tranquart, A. Bouakaz, Characterization of cell membrane response to ultrasound activated microbubbles, IEEE Trans. Ultrason. Ferroelectr. Freq. Control 55 (2008) 44–49.
[80] T.A. Tran, S. Roger, J.Y. Le Guennec, F. Tranquart, A. Bouakaz, Effect of ultrasound-activated microbubbles on the cell electrophysiological properties, Ultrasound Med. Biol. 33 (2007) 158–163.
[81] L.J.M. Juffermans, O. Kamp, P.A. Dijkmans, C.A. Visser, R.J.P. Musters, Low-intensity ultrasound-exposed microbubbles provoke local hyperpolarization of the cell membrane via activation of BKCa channels, Ultrasound Med. Biol. 34 (2008) 502–508.
[82] M. Afadzi, S.P. Strand, E.A. Nilssen, S.E. Masoy, T.F. Johansen, R. Hansen, B.A. Angelsen, C.D. Davies, Mechanisms of the ultrasound-mediated intracellular delivery of liposomes and dextrans, IEEE Trans. Ultrason. Ferroelectr. Freq. Control 60 (2013) 21–33.
[83] N. Mizrahi, E.H.H. Zhou, G. Lenormand, R. Krishnan, D. Weihs, J.P. Butler, D.A. Weitz, J.J. Fredberg, E. Kimmel, Low intensity ultrasound perturbs cytoskeleton dynamics, Soft Matter 8 (2012) 2438–2443.
[84] S. Zhang, J.Q. Cheng, Y.X. Qin, Mechanobiological modulation of cytoskeleton and calcium influx in osteoblastic cells by short-term focused acoustic radiation force, PLoS One 7 (2012).
[85] L.J.M. Juffermans, A. van Dijk, C.A.M. Jongenelen, B. Drukarch, A. Reijerkerk, H.E. de Vries, O. Kamp, R.J.P. Musters, Ultrasound and microbubble-induced intra- and intercellular bioeffects in primary endothelial cells, Ultrasound Med. Biol. 35 (2009) 1917–1927.
[86] X. Chen, R.S. Leow, Y.X. Hu, J.M.F. Wan, A.C.H. Yu, Single-site sonoporation disrupts actin cytoskeleton organization, J. R. Soc. Interface 11 (2014).
[87] H.R. Guzman, D.X. Nguyen, S. Khan, M.R. Prausnitz, Ultrasound-mediated disruption of cell membranes. II. Heterogeneous effects on cells, J. Acoust. Soc. Am. 110 (2001) 597–606.
[88] K. Saito, K. Miyake, P.L. McNeil, K. Kato, K. Yago, N. Sugai, Plasma membrane disruption underlies injury of the corneal endothelium by ultrasound, Exp. Eye Res. 68 (1999) 431–437.
[89] P.L. McNeil, R.A. Steinhardt, Loss, restoration, and maintenance of plasma membrane integrity, J. Cell Biol. 137 (1997) 1–4.
[90] P.L. McNeil, R.A. Steinhardt, Plasma membrane disruption: repair, prevention, adaptation, Annu. Rev. Cell Dev. Biol. 19 (2003) 697–731.
[91] N.W. Andrews, M. Corrotte, T. Castro-Gomes, Above the fray: surface remodeling by secreted lysosomal enzymes leads to endocytosis-mediated plasma membrane repair, Semin. Cell Dev. Biol. 45 (2015) 2–9.
[92] R.K. Schlicher, H. Radhakrishna, T.P. Tolentino, R.P. Apkarian, V. Zarnitsyn, M.R. Prausnitz, Mechanism of intracellular delivery by acoustic cavitation, Ultrasound Med. Biol. 32 (2006) 915–924.
[93] A. Reddy, E.V. Caler, N.W. Andrews, Plasma membrane repair is mediated by Ca (2 +)-regulated exocytosis of lysosomes, Cell 106 (2001) 157–169.
[94] F. Yang, N. Gu, D. Chen, X. Xi, D. Zhang, Y. Li, J. Wu, Experimental study on cell self-sealing during sonoporation, J. Control. Release 131 (2008) 205–210.
[95] A. Draeger, K. Monastyrskaya, E.B. Babiychuk, Plasma membrane repair and cellular damage control: the annexin survival kit, Biochem. Pharmacol. 81 (2011) 703–712.
[96] V. Idone, C. Tam, J.W. Goss, D. Toomre, M. Pypaert, N.W. Andrews, Repair of injured plasma membrane by rapid Ca2 + -dependent endocytosis, J. Cell Biol. 180 (2008) 905–914.
[97] C. Tam, V. Idone, C. Devlin, M.C. Fernandes, A. Flannery, X.X. He, E. Schuchman, I. Tabas, N.W. Andrews, Exocytosis of acid sphingomyelinase by wounded cells promotes endocytosis and plasma membrane repair, J. Cell Biol. 189 (2010) 1027–1038.
[98] P. Saftig, J. Klumperman, Lysosome biogenesis and lysosomal membrane proteins: trafficking meets function, Nat. Rev. Mol. Cell Biol. 10 (2009) 623–635.
[99] G. Apodaca, Modulation of membrane traffic by mechanical stimuli, Am. J. Physiol. Ren. Physiol. 282 (2002) F179–190.
[100] J. Hauser, M. Hauser, G. Muhr, S. Esenwein, Ultrasound-induced modifications of cytoskeletal components in osteoblast-like SAOS-2 cells, J. Orthop. Res. 27 (2009) 286–294.
[101] R.S. Leow, J.M.F. Wan, A.C.H. Yu, Membrane blebbing as a recovery manoeuvre in site-specific sonoporation mediated by targeted microbubbles, J. R. Soc. Interface 12 (2015).
[102] H. Chen, A.A. Brayman, W. Kreider, M.R. Bailey, T.J. Matula, Observations of translation and jetting of ultrasound-activated microbubbles in mesenteric microvessels, Ultrasound Med. Biol. 37 (2011) 2139–2148.
[103] H. Chen, A.A. Brayman, A.P. Evan, T.J. Matula, Preliminary observations on the spatial correlation between short-burst microbubble oscillations and vascular bioeffects, Ultrasound Med. Biol. 38 (2012) 2151–2162.
[104] H. Chen, W. Kreider, A.A. Brayman, M.R. Bailey, T.J. Matula, Blood vessel deformations on microsecond time scales by ultrasonic cavitation, Phys. Rev. Lett. 106 (2011).
[105] E.E. Konofagou, Optimization of the ultrasound-induced blood-brain barrier opening, Theranostics 2 (2012) 1223–1237.
[106] J. Park, Y.Z. Zhang, N. Vykhodtseva, F.A. Jolesz, N.J. McDannold, The kinetics of blood brain barrier permeability and targeted doxorubicin delivery into brain induced by focused ultrasound, J. Control. Release 162 (2012) 134–142.
[107] N. Sheikov, N. McDannold, S. Sharma, K. Hynynen, Effect of focused ultrasound applied with an ultrasound contrast agent on the tight junctional integrity of the brain microvascular endothelium, Ultrasound Med. Biol. 34 (2008) 1093–1104.
[108] J.Y. Park, Y.Z. Zhang, N. Vykhodtseva, J.D. Akula, N.J. McDannold, Targeted and reversible blood-retinal barrier disruption via focused ultrasound and microbubbles, PLoS One 7 (2012).
[109] K. Hynynen, N. McDannold, N. Vykhodtseva, F.A. Jolesz, Noninvasive MR imaging-guided focal opening of the blood-brain barrier in rabbits, Radiology 220 (2001) 640–646.
[110] G.P. Howles, K.F. Bing, Y. Qi, S.J. Rosenzweig, K.R. Nightingale, G.A. Johnson, Contrast-enhanced in vivo magnetic resonance microscopy of the mouse brain enabled by noninvasive opening of the blood-brain barrier with ultrasound, Magn. Reson. Med. 64 (2010) 995–1004.
[111] N. McDannold, C.D. Arvanitis, N. Vykhodtseva, M.S. Livingstone, Temporary disruption of the blood-brain barrier by use of ultrasound and microbubbles: safety and efficacy evaluation in rhesus macaques, Cancer Res. 72 (2012) 3652–3663.
[112] D. Mehta, A.B. Malik, Signaling mechanisms regulating endothelial permeability, Physiol. Rev. 86 (2006) 279–367.
[113] S.K. Nigam, E. Rodriguezboulan, R.B. Silver, Changes in intracellular calcium during the development of epithelial polarity and junctions, Proc. Natl. Acad. Sci. U. S. A. 89 (1992) 6162–6166.
[114] R.O. Stuart, A. Sun, K.T. Bush, S.K. Nigam, Dependence of epithelial intercellular junction biogenesis on thapsigargin-sensitive intracellular calcium stores, J. Biol. Chem. 271 (1996) 13636–13641.

[115] R.C. Brown, T.P. Davis, Calcium modulation of adherens and tight junction function - a potential mechanism for blood-brain barrier disruption after stroke, Stroke 33 (2002) 1706–1711.
[116] N.J. Abbott, Role of intracellular calcium in regulation of brain endothelial permeability, Introduction to the Blood-Brain Barrier: Methodology, Biology and Pathology, Cambridge University Press, NY, USA, 1998, pp. 341–351.
[117] J. Park, Z. Fan, C.X. Deng, Effects of shear stress cultivation on cell membrane disruption and intracellular calcium concentration in sonoporation of endothelial cells, J. Biomech. 44 (2011) 164–169.
[118] N. Sheikov, N. McDannold, N. Vykhodtseva, F. Jolesz, K. Hynynen, Cellular mechanisms of the blood-brain barrier opening induced by ultrasound in presence of microbubbles, Ultrasound Med. Biol. 30 (2004) 979–989.
[119] J. Deng, Q. Huang, F. Wang, Y. Liu, Z. Wang, Z. Wang, Q. Zhang, B. Lei, Y. Cheng, The role of caveolin-1 in blood-brain barrier disruption induced by focused ultrasound combined with microbubbles, J. Mol. Neurosci. 46 (2012) 677–687.
[120] S.M. Dudek, J.G.N. Garcia, Cytoskeletal regulation of pulmonary vascular permeability, J. Appl. Physiol. 91 (2001) 1487–1500.
[121] Z.M. Goeckeler, R.B. Wysolmerski, Myosin light-chain kinase-regulated endothelial-cell contraction - the relationship between isometric tension, actin polymerization, and myosin phosphorylation, J. Cell Biol. 130 (1995) 613–627.
[122] J. Waschke, F.E. Curry, R.H. Adamson, D. Drenckhahn, Regulation of actin dynamics is critical for endothelial barrier functions, Am. J. Phys. Heart Circ. Phys. 288 (2005) H1296–1305.
[123] B. Wojciak-Stothard, S. Potempa, T. Eichholtz, A.J. Ridley, Rho and Rac but not Cdc42 regulate endothelial cell permeability, J. Cell Sci. 114 (2001) 1343–1355.
[124] L. Gonzalez-Mariscal, A. Betanzos, A. Avila-Flores, MAGUK proteins: structure and role in the tight junction, Semin. Cell Dev. Biol. 11 (2000) 315–324.
[125] Q. Yao, J. Chen, H. Cao, J.D. Orth, J.M. McCaffery, R.-V. Stan, M.A. McNiven, Caveolin-1 interacts directly with dynamin-2, J. Mol. Biol. 348 (2005) 491–501.
[126] T. Hirase, S. Kawashima, E.Y. Wong, T. Ueyama, Y. Rikitake, S. Tsukita, M. Yokoyama, J.M. Staddon, Regulation of tight junction permeability and occludin phosphorylation by Rhoa-p160ROCK-dependent and -independent mechanisms, J. Biol. Chem. 276 (2001) 10423–10431.
[127] A.A. Birukova, K.G. Birukov, K. Smurova, D. Adyshev, K. Kaibuchi, I. Alieva, J.G.N. Garcia, A.D. Verin, Novel role of microtubules in thrombin-induced endothelial barrier dysfunction, FASEB J. 18 (2004) 1879–1890.
[128] M. Gorovoy, J.X. Niu, O. Bernard, J. Profirovic, R. Minshall, R. Neamu, T. Voyno-Yasenetskaya, LIM kinase 1 coordinates microtubule stability and actin polymerization in human endothelial cells, J. Biol. Chem. 280 (2005) 26533–26542.
[129] I. Petrache, A. Birukova, S.I. Ramirez, J.G.N. Garcia, A.D. Verin, The role of the microtubules in tumor necrosis factor-alpha-induced endothelial cell permeability, Am. J. Respir. Cell Mol. 28 (2003) 574–581.
[130] J. Yu, S. Bergaya, T. Murata, I.F. Alp, M.P. Bauer, M.I. Lin, M. Drab, T.V. Kurzchalia, R.V. Stan, W.C. Sessa, Direct evidence for the role of caveolin-1 and caveolae in mechanotransduction and remodeling of blood vessels, J. Clin. Invest. 116 (2006) 1284–1291.
[131] J.T. Sutton, K.J. Haworth, G. Pyne-Geithman, C.K. Holland, Ultrasound-mediated drug delivery for cardiovascular disease, Expert Opin. Drug Deliv. 10 (2013) 573–592.
[132] A.J. Ridley, Rho family proteins and regulation of the actin cytoskeleton, Prog. Mol. Subcell. Biol. 22 (1999) 1–22.
[133] B. Wojciak-Stothard, A.J. Ridley, Rho GTPases and the regulation of endothelial permeability, Vasc. Pharmacol. 39 (2002) 187–199.
[134] V. Vouret-Craviari, C. Bourcier, E. Boulter, E. Van Obberghen-Schilling, Distinct signals via Rho GTPases and Src drive shape changes by thrombin and sphingosine-1-phosphate in endothelial cells, J. Cell Sci. 115 (2002) 2475–2484.
[135] D. Mehta, C. Tiruppathi, R. Sandoval, R.D. Minshall, M. Holinstat, A.B. Malik, Modulatory role of focal adhesion kinase in regulating human pulmonary arterial endothelial barrier function, J. Physiol. Lond. 539 (2002) 779–789.
[136] S.K. Quadri, M. Bhattacharjee, K. Parthasarathi, T. Tanita, J. Bhattacharya, Endothelial barrier strengthening by activation of focal adhesion kinase, J. Biol. Chem. 278 (2003) 13342–13349.
[137] P. Kouklis, M. Konstantoulaki, S. Vogel, M. Broman, A.B. Malik, Cdc42 regulates the restoration of endothelial barrier function, Circ. Res. 94 (2004) 159–166.
[138] D. Mehta, M. Konstantoulaki, G.U. Ahmmed, A.B. Malik, Sphingosine 1-phosphate-induced mobilization of intracellular Ca2 + mediates Rac activation and adherens junction assembly in endothelial cells, J. Biol. Chem. 280 (2005) 17320–17328.
[139] J.M. Taylor, M.M. Macklem, J.T. Parsons, Cytoskeletal changes induced by GRAF, the GTPase regulator associated with focal adhesion kinase, are mediated by Rho, J. Cell Sci. 112 (Pt 2) (1999) 231–242.
[140] N.K. Noren, W.T. Arthur, K. Burridge, Cadherin engagement inhibits RhoA via p190RhoGAP, J. Biol. Chem. 278 (2003) 13615–13618.
[141] W.T. Arthur, L.A. Petch, K. Burridge, Integrin engagement suppresses RhoA activity via a c-Src-dependent mechanism, Curr. Biol. 10 (2000) 719–722.
[142] C.E. Patterson, H. Lum, K.L. Schaphorst, A.D. Verin, J.G.N. Garcia, Regulation of endothelial barrier function by the cAMP-dependent protein kinase, Endothelium 7 (2000) 287.
[143] K.M. Comerford, D.W. Lawrence, K. Synnestvedt, B.P. Levi, S.P. Colgan, Role of vasodilator-stimulated phosphoprotein in PKA-induced changes in endothelial junctional permeability, FASEB J. 16 (2002) 583–585.
[144] M. Derieppe, K. Rojek, J.M. Escoffre, B.D. de Senneville, C. Moonen, C. Bos, Recruitment of endocytosis in sonopermeabilization-mediated drug delivery: a real-time study, Phys. Biol. 12 (2015) 046010.
[145] S. Tardoski, E. Gineyts, J. Ngo, A. Kocot, P. Clezardin, D. Melodelima, Low-intensity ultrasound promotes clathrin-dependent endocytosis for drug penetration into tumor cells, Ultrasound Med. Biol. 41 (2015) 2740–2754.
[146] F. Fekri, R.C. Delos Santos, R. Karshafian, C.N. Antonescu, Ultrasound microbubble treatment enhances clathrin-mediated endocytosis and fluid-phase uptake through distinct mechanisms, PLoS One 11 (2016).
[147] D.M.B. de Paula, V.B. Valero-Lapchik, E.J. Paredes-Gamero, S.W. Han, Therapeutic ultrasound promotes plasmid DNA uptake by clathrin-mediated endocytosis, J. Gene Med. 13 (2011) 392–401.
[148] G. Basta, L. Venneri, G. Lazzerini, E. Pasanisi, M. Pianelli, N. Vesentini, S. Del Turco, C. Kusmic, E. Picano, In vitro modulation of intracellular oxidative stress of endothelial cells by diagnostic cardiac ultrasound, Cardiovasc. Res. 58 (2003) 156–161.
[149] V. Lioneiti, A. Fittipaldi, S. Agostini, M. Giacca, F.A. Recchia, E. Picano, Enhanced caveolae-mediated endocytosis by diagnostic ultrasound in vitro, Ultrasound Med. Biol. 35 (2009) 136–143.
[150] M. Corrotte, M.C. Fernandes, C. Tam, N.W. Andrews, Toxin pores endocytosed during plasma membrane repair traffic into the lumen of MVBs for degradation, Traffic 13 (2012) 483–494.
[151] M. Postema, A. Van Wamel, C.T. Lancee, N. De Jong, Ultrasound-induced encapsulated microbubble phenomena, Ultrasound Med. Biol. 30 (2004) 827–840.
[152] A.P. Sarvazyan, O.V. Rudenko, W.L. Nyborg, Biomedical applications of radiation force of ultrasound: historical roots and physical basis, Ultrasound Med. Biol. 36 (2010) 1379–1394.
[153] P. Palanchon, P. Tortoli, A. Bouakaz, M. Versluis, N. de Jong, Optical observations of acoustical radiation force effects on individual air bubbles, IEEE Trans. Ultrason. Ferroelectr. Freq. Control 52 (2005) 104–110.
[154] S. Kotopoulis, M. Postema, Microfoam formation in a capillary, Ultrasonics 50 (2010) 260–268.
[155] B. Han, X.H. Bai, M. Lodyga, J. Xu, B.B. Yang, S. Keshavjee, M. Post, M.Y. Liu, Conversion of mechanical force into biochemical signaling, J. Biol. Chem. 279 (2004) 54793–54801.
[156] E.S. Statnikov, O.V. Korolkov, V.N. Vityazev, Physics and mechanism of ultrasonic impact, Ultrasonics 44 (2006) E533–E538.
[157] Z. Fan, Y. Sun, C. Di, D. Tay, W. Chen, C.X. Deng, J. Fu, Acoustic tweezing cytometry for live-cell subcellular modulation of intracellular cytoskeleton contractility, Sci. Rep. 3 (2013) 2176.
[158] N.P. Whitney, A.C. Lamb, T.M. Louw, A. Subramanian, Integrin-mediated mechanotransduction pathway of low-intensity continuous ultrasound in human chondrocytes, Ultrasound Med. Biol. 38 (2012) 1734–1743.
[159] M. Sato, K. Nagata, S. Kuroda, S. Horiuchi, T. Nakamura, M. Karima, T. Inubushi, E. Tanaka, Low-intensity pulsed ultrasound activates integrin-mediated mechanotransduction pathway in synovial cells, Ann. Biomed. Eng. 42 (2014) 2156–2163.
[160] T.M. Louw, G. Budhiraja, H.J. Viljoen, A. Subramanian, Mechanotransduction of ultrasound is frequency dependent below the cavitation threshold, Ultrasound Med. Biol. 39 (2013) 1303–1319.
[161] D.I. Mundy, T. Machleidt, Y.S. Ying, R.G.W. Anderson, G.S. Bloom, Dual control of caveolar membrane traffic by microtubules and the actin cytoskeleton, J. Cell Sci. 115 (2002) 4327–4339.
[162] R.K. Schlicher, J.D. Hutcheson, H. Radhakrishna, R.P. Apkarian, M.R. Prausnitz, Changes in cell morphology due to plasma membrane wounding by acoustic cavitation, Ultrasound Med. Biol. 36 (2010) 677–692.
[163] H. Grassme, J. Riethmuller, E. Gulbins, Biological aspects of ceramide-enriched membrane domains, Prog. Lipid Res. 46 (2007) 161–170.
[164] J.M. Holopainen, M.I. Angelova, P.K.J. Kinnunen, Vectorial budding of vesicles by asymmetrical enzymatic formation of ceramide in giant liposomes, Biophys. J. 78 (2000) 830–838.
[165] J.D. Hutcheson, R.K. Schlicher, H.K. Hicks, M.R. Prausnitz, Saving cells from ultrasound-induced apoptosis: quantification of cell death and uptake following sonication and effects of targeted calcium chelation, Ultrasound Med. Biol. 36 (2010) 1008–1021.
[166] V. Lariccia, M. Fine, S. Magi, M.J. Lin, A. Yaradanakul, M.C. Llaguno, D.W. Hilgemann, Massive calcium-activated endocytosis without involvement of classical endocytic proteins, J. Gen Physiol. 137 (2011) 111–132.
[167] D. Vercauteren, R.E. Vandenbroucke, A.T. Jones, J. Rejman, J. Demeester, S.C. De Smedt, N.N. Sanders, K. Braeckmans, The use of inhibitors to study endocytic pathways of gene carriers: optimization and pitfalls, Mol. Ther. 18 (2010) 561–569.
[168] A. Delalande, C. Leduc, P. Midoux, M. Postema, C. Pichon, Efficient gene delivery by sonoporation is associated with microbubble entry into cells and the clathrin-dependent endocytosis pathway, Ultrasound Med. Biol. 41 (2015) 1913–1926.
[169] S. Ibsen, C.E. Schutt, S. Esener, Microbubble-mediated ultrasound therapy: a review of its potential in cancer treatment, Drug Des. Dev. Ther. 7 (2013) 375–388.
[170] R.H. Perera, C. Hernandez, H.Y. Zhou, P. Kota, A. Burke, A.A. Exner, Ultrasound imaging beyond the vasculature with new generation contrast agents, Wires Nanomed. Nanobiol. 7 (2015) 593–608.
[171] C. Desjouy, A. Poizat, B. Gilles, C. Inserra, J.C. Bera, Control of inertial acoustic cavitation in pulsed sonication using a real-time feedback loop system, J. Acoust. Soc. Am. 134 (2013) 1640–1646.
[172] A.N. Pouliopoulos, S. Bonaccorsi, J.J. Choi, Exploiting flow to control the in vitro spatiotemporal distribution of microbubble-seeded acoustic cavitation activity in ultrasound therapy, Phys. Med. Biol. 59 (2014) 6941–6957.
[173] C. Coviello, R. Kozick, J. Choi, M. Gyongy, C. Jensen, P.P. Smith, C.C. Coussios, Passive acoustic mapping utilizing optimal beamforming in ultrasound therapy monitoring, J. Acoust. Soc. Am. 137 (2015) 2573–2585.